

1  
2  
3  
4  
5  
6  
7  
8  
9  
10  
11  
12  
13  
14  
15  
16  
17  
18  
19  
20  
21  
22

Measurement report: Impact of domestic heating on dust  
deposition sources in hyper-arid Qaidam Basin, northern  
Qinghai-Xizang Plateau

Haixia Zhu<sup>abc</sup>, Lufei Zhen<sup>abc</sup>, Suping Zhao<sup>d\*</sup>, Xiying Zhang<sup>ab\*</sup>

*<sup>a</sup> Key Laboratory of Green and High-end Utilization of Salt Lake Resources, Qinghai Institute of Salt Lakes, Chinese Academy of Sciences, Xining, 810008, China.*  
*<sup>b</sup> Qinghai Provincial Key Laboratory of Geology and Environment of Salt Lakes, Qinghai Institute of Salt Lakes, Chinese Academy of Sciences, Xining, 810008, China.*  
*<sup>c</sup> University of the Chinese Academy of Sciences, Beijing, 100049, China*  
*<sup>d</sup> Key Laboratory of Cryospheric Science and Frozen Soil Engineering, Northwest Institute of Eco-Environment and Resources, Chinese Academy of Sciences, Lanzhou, 730000, China*  
*\* Corresponding author. E-mail address: xyzhchina@isl.ac.cn (Xiying Zhang) and zhaosp@lzb.ac.cn (Suping Zhao)*

23 **Highlights**

24 1. The temporal and spatial distribution of carbonaceous aerosols was analyzed using various carbon  
25 indicators.

26 2. Domestic heating significantly increased atmospheric pollutants in rural areas.

27 3. The unique energy structure in Qaidam Basin significantly influenced the glaciers of the  
28 Qinghai-Xizang Plateau and should not be overlooked.

29

30 **Abstract**

31 Given the unique energy profile of the Qaidam Basin (QDB), it is crucial to examine the impacts of  
32 domestic heating on the Qinghai-Xizang Plateau (QXP) and global atmospheric systems. This study  
33 collected monthly dust deposition at six sites in the southern QDB between 2020 and 2023. We  
34 identified the sources of dust-fall during domestic heating (HP) and non-heating periods (NHP) in  
35 urban and rural areas and its environmental effects. The results demonstrated that domestic heating  
36 increased the concentration of water-soluble ions in rural areas, trace elements in urban areas, and  
37 carbon emissions in both. Among various carbon indicators, organic carbon (OC) and element  
38 carbon (EC) levels rose during the HP, with Char-EC as the primary component of EC (80.44%).  
39 Char-EC concentrations were higher in urban areas (85.00%), while secondary organic carbon  
40 (68.17%), the main contributor to OC, was more prevalent in rural (73.92%). The OC/EC ratio in  
41 urban areas remained stable with an average of 2.16. In contrast, the rural OC/EC ratio was  
42 significantly higher during the NHP ( $7.27 \pm 4.66$ ) than during the HP ( $4.57 \pm 3.02$ ). Additionally,  
43 the char/soot ratio was elevated in the HP ( $5.06 \pm 4.08$ ) compared to the NHP ( $4.42 \pm 3.09$ ). The  
44 OC/EC and char-EC/soot-EC ratios, along with PMF results, indicated that coal combustion  
45 (17.28%) and biomass burning (32.50%) were the main contributors to dust deposition in rural areas,  
46 strongly influenced by domestic heating, whereas urban dust predominantly originated from traffic  
47 (44.43%) and industrial emissions (16.41%). Coal consumption in QDB was greater during the HP  
48 than that of other dust sources in the QXP. This increased consumption leads to higher emissions of  
49 atmospheric pollution, which may accelerate glacier melting in the region. Consequently,  
50 integrating QDB carbon aerosols into future environmental policies and climate models for the QXP  
51 is essential. This study provides a reference for investigating carbonaceous aerosols in climatically  
52 similar hyper-arid basins with intensive human activity and salt lake regions.

53 **Keywords:** Qinghai-Xizang Plateau; Qaidam Basin; Biomass burning; carbonaceous elements;  
54 atmospheric dust deposition.

55

56 **Short summary**

57 This study collected dust samples from six sites in the Qaidam Basin over three years to investigate  
58 the impact of domestic heating on atmospheric dust in hyper-arid region. Our results indicate that  
59 rural dust is significantly influenced by heating, particularly from coal and biomass burning, which  
60 accounts for over 70% of total sources. The unique energy structure here has resulted in distinct  
61 environmental effects from the emitted carbonaceous aerosols and useful for similar dry areas.

## 62 **1. Introduction**

63 Atmospheric dust, a critical component of particulate matter (PM), serves as both an air quality  
64 indicator and environmental stressor, influencing hydrological cycles and soil ecosystems (Feng et  
65 al., 2019). Recent advancements in understanding PM characteristics—particularly chemical  
66 composition (e.g. water-soluble ions, organic carbon, and elemental carbon) and source  
67 apportionment—have been achieved through principal component analysis (PCA), chemical mass  
68 balance (CMB), and positive matrix factorization (PMF) models (Lai et al., 2016; Yao et al., 2016;  
69 Zhang et al., 2015a). PMF analysis of atmospheric dust in urban areas such as Lanzhou, Taiyuan,  
70 and Jinan have identified diverse sources, including coal combustion, industrial emissions,  
71 construction dust, windblown dust, vehicle emissions, and resuspended road dust. Seasonal  
72 variations indicate that coal combustion during the domestic heating period and regional  
73 meteorological conditions significantly influence dust deposition (Hu and Liu, 2022; Chen et al.,  
74 2024; Yang et al., 2024; Zhang et al., 2022). These findings underscore the urgency of region-  
75 specific pollution control strategies.

76 The Qinghai-Xizang Plateau (QXP) is a key regulator of Northern Hemisphere climate  
77 variability and plays a vital role in global ecological and climatic stability, often referred to as the  
78 “Asian Water Tower” (Liu et al., 2019; Liu et al., 2020b). However, rapid glacier retreat on the  
79 plateau poses risks to the Asian hydrological cycle and the monsoon system, with potential adverse  
80 impacts if unchecked (Luo et al., 2020). Beyond climate warming and increased humidity, black  
81 carbon (BC) significantly accelerates glacial melt by inducing atmospheric warming and enhancing  
82 radiative absorption at the glacier surface (Bond and Bergstrom, 2006; Chen et al., 2015). Notably,  
83 biomass burning in South and Central Asia during winter serves as a major source of BC, further  
84 exacerbating glacier decline on the plateau (Zhang et al., 2015b; Zheng et al., 2017; Xu et al., 2018b).  
85 However, local sources within the QTP, particularly the Qaidam Basin (QDB) in the northeastern  
86 region, should not be underestimated, as QDB is a key dust source for the plateau (Wei et al., 2017;  
87 Zheng et al., 2021).

88 The QDB, known as the “Treasure Bowl” of the QXP, is rich in minerals, coal, oil, and gas,  
89 positioning it as a key economic hub in northwest China. It has a high population density and intense  
90 human activity, yet it is highly sensitive to climate change. Extensive resource extraction has

91 rendered its ecosystem fragile (Li and Sha, 2022), exacerbating atmospheric pollution. Unlike South  
92 Asia, Central Asia, and Xizang—where biomass fuels dominate—QDB relies primarily on a  
93 mixture of coal, yak dung, and firewood for winter domestic heating, reflecting a unique energy  
94 structure (Liu et al., 2008; Xiao et al., 2015; Behera et al., 2015; Kerimray et al., 2018; Jiang et al.,  
95 2020; Shen et al., 2021). The combustion of coal releases significant pollutants, light-absorbing  
96 organic compounds like BC and brown carbon, and hazardous gases such as carbon dioxide (CO<sub>2</sub>),  
97 nitrogen oxides (NO<sub>x</sub>) and carbon monoxide (CO). These emissions impact human health and  
98 exacerbate climate warming, thereby influencing regional and global climate systems (Munawer,  
99 2018; Ye et al., 2020; Zhou et al., 2025). Consequently, we posit that seasonal carbon emissions in  
100 QDB, particularly during winter domestic heating, could exert a unique influence on the climate  
101 and ecological stability of the QXP.

102         Additionally, the QDB as a representative arid region with intensive human activity, exhibits  
103 climatic and environmental conditions comparable to the Tarim and Junggar Basins in Xinjiang, the  
104 Great Basin in the United States, and other hyper-arid areas. These regions are characterized by low  
105 precipitation, rich mineral resources subject to significant anthropogenic impact, and abundant salt  
106 lakes. Similarly, salt lakes such as the Uyuni in Bolivia, Atacama in Chile, and Ombre-Muerto in  
107 Argentina are located on high plateaus averaging 3,000 m in elevation, with surrounding climates  
108 and environments comparable to those of the QDB. Research in the Tarim and Junggar Basins has  
109 predominantly focused on dust events, their sources, and associated gas emissions (Gao and  
110 Washington, 2010; Liu et al., 2016b; Filonchik et al., 2018; Yu et al., 2019; Zhou et al., 2023). In  
111 the Great Basin, studies largely address ozone and dust sources (Hahnenberger and Nicoll, 2012;  
112 Vancuren and Gustin, 2015; Miller et al., 2015). Research on salt lake atmospheres has  
113 predominantly focused on high-salinity dust emissions resulting from lakebed desiccation due to  
114 resource extraction (L w et al., 2013; Gholampour et al., 2015; Moravek et al., 2019; Christie et al.,  
115 2025), with limited research on atmospheric carbon components, their sources, and environmental  
116 impacts. Therefore, this research aims to investigate atmospheric carbonaceous aerosols in arid  
117 basins with intensive human activity and climates comparable to the QDB, as well as in salt lakes  
118 environments.

119         This study, conducted from January 2020 to March 2023, involved monthly dust deposition  
120 sampling at six urban and rural monitoring sites located in the southern QDB. Samples were

121 categorized into two seasonal periods: the domestic heating (HP) and the non-domestic heating  
122 (NHP) periods. The HYSPLIT model, and PMF receptor modeling using analyses of dust flux,  
123 soluble ions, trace elements, and carbonaceous components, alongside OC/EC and char/soot  
124 ratios—the primary sources of dust deposition were identified, with particular emphasis on  
125 contributions from domestic heating. The study further evaluated the environmental impacts on the  
126 QXP, considering its distinctive energy structure. Furthermore, these findings offer a scientific basis  
127 and reference for examining atmospheric carbonaceous aerosols in arid basins with similar climates  
128 and human activities to the QDB, as well as in salt lake regions.

129

## 130 **2. Materials and methods**

### 131 **2.1 Sampling**

132 The QDB, situated in the northeastern part of the QXP, is bordered by the Altyn-Tagh, Kunlun,  
133 and Qilian mountains, making it one of China's largest intermontane basins (Zhang, 1987). With an  
134 average elevation of 3,000 m, the basin features an extremely arid climate characterized by less than  
135 20 mm of annual precipitation in the northwestern region, while evaporation rates exceed 2,000 mm.  
136 The QDB is rich in salt lakes, non-ferrous metals, and hydrocarbon resources, with significant coal  
137 deposits. It leads China in reserves of halite, potash, magnesium, lithium, strontium, asbestos,  
138 earning it the nickname “Treasure Basin”. As a major salt lake resource area, it hosts 33 lakes—  
139 including Qarhan, Dachaidan, and Caka Salt Lake—and faces notable conflicts between resource  
140 extraction and ecological preservation. Agriculturally, it cultivates crops like goji berries, quinoa,  
141 and forage grass, and hosts China’s largest resource-rich circular economy pilot zone. The  
142 permanent population of the basin is approximately 400,000, primarily using coal, yak dung, and  
143 firewood for domestic heating (Jiang et al., 2020). Additionally, annual tourism peaks from May to  
144 September, attracting around 17 million visitors, which likely amplifies atmospheric pollutant  
145 emissions.

146 From January 2020 to March 2023, monthly dust deposition samples were collected from six  
147 monitoring stations in the southern QDB. The stations included Xiao Zaohuo (XZH), Golmud  
148 (GEM), Da Gele (LTC), Nuo Muhong (NMH), Balong (BLX), and Dulan station (DLX). Dry  
149 deposition collection employed the glass ball method using Marble dust collector (MDCO) designed

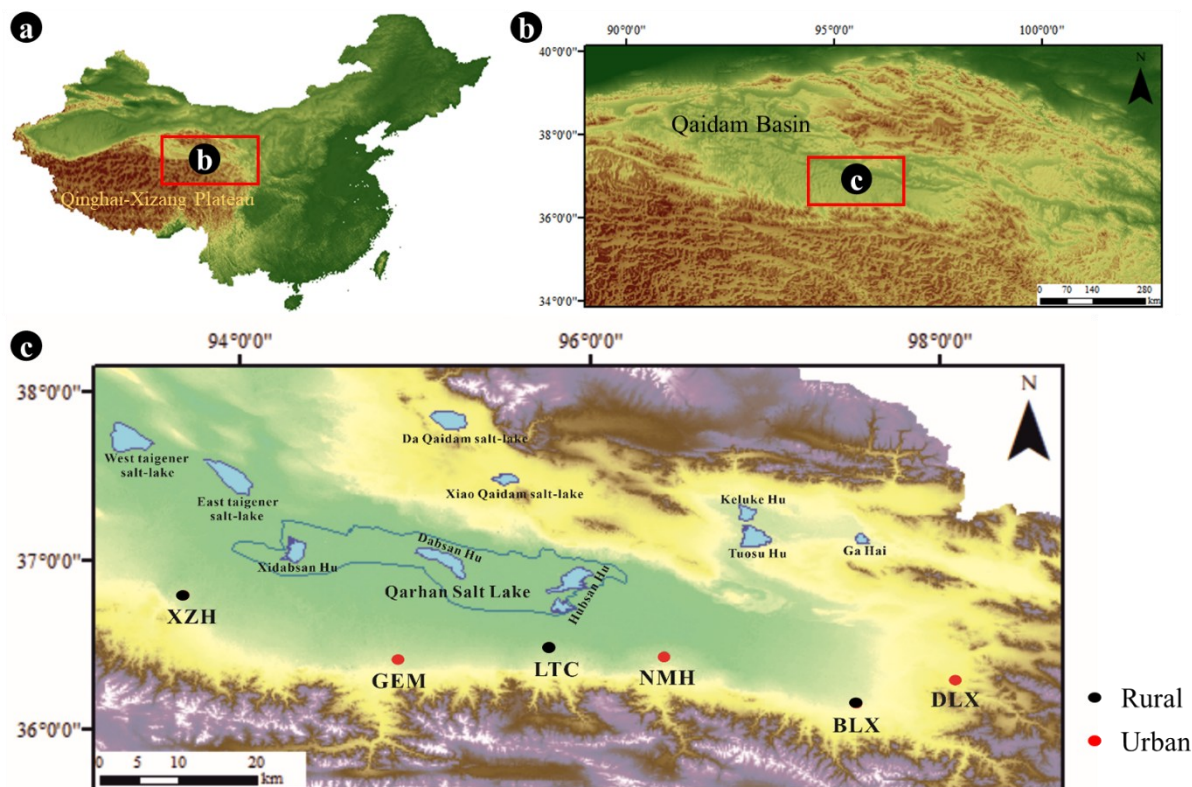
150 dust collection cylinders (Sow et al., 2006). The stainless steel collection device (50×30×30 cm)  
151 contained a plastic sieve container of identical dimensions, with the sieve base positioned 10 cm  
152 above the opening and perforated with 0.5 cm diameter holes (Figure S1). To minimize dust  
153 resuspension during high wind events (Qian and Dong, 2004), two layers of 16 mm glass balls were  
154 placed within the sieve container. A high-density polyethylene bag was attached to the base for  
155 sample collection. According to Sow et al (2006), the collection efficiency of the MDCO decreases  
156 with increasing wind speed, dropping below 20% when wind speed exceeds 3 m/s, and it  
157 preferentially collects fine dust particles ranging from 10 to 31 μm in size (Chow, 1995). This type  
158 of collector has been widely used in many studies to evaluate local dust conditions (Abdollahi et al.,  
159 2021; Barjoe et al., 2021; Alzahrani et al., 2024). Therefore, we consider this collector effective  
160 for capturing fine dust particles, and the actual dust deposition flux can be estimated by accounting  
161 for its approximately 20% collection efficiency.

162 In this study, dust samples were collected monthly, with each sampling period lasting 30 or 31  
163 days. The installation height and environment of the samplers are provided in Table S1. To ensure  
164 only dry dust was collected, collection devices were covered during rain or snowfall. A total of 37,  
165 39, 23, 30, 16, and 29 samples were obtained from XZH, GEM, LTC, NMH, BLX, and DLX stations,  
166 respectively. Laboratory protocols incorporated biannual analyses with negative controls and  
167 appropriate control samples. As continuous dust monitoring commenced in 2020, site blanks were  
168 evaluated during initial sampling. Stations were classified as Urban (GEM, NMH, DLX) and Rural  
169 (XZH, LTC, BLX) based on location characteristics. Consistent with the cold-arid climate in QDB,  
170 the HP was defined as October-April, while the NHP spanned May-September.

171 Materials such as plant remnants, microfauna, and bird droppings were removed from the  
172 sample bags with tweezers. The samples were then measured on a balance (0.0001 g) to determine  
173 the dust deposition flux (Eq. 1) (Yu et al., 2016):

$$174 \quad M = \frac{m \times 30}{S \times K}, \quad (1)$$

175 where M is dust deposition [g/(m<sup>2</sup>·30d)]; m is the sample mass (g); S is the area of the dust collection  
176 device (m<sup>2</sup>); and K is the actual number of sampling days per month (d).



177

178 **Figure 1.** Spatial distribution of monitoring stations in the southern Qaidam Basin. Urban stations  
 179 (red) and rural stations (black) are labeled as follows: XZH (Xiao Zaohuo), GEM (Golmud), LTC  
 180 (Da Gele), NMH (Nuo Muhong), BLX (Balong), DLX (Dulan).

181

## 182 2.2 Water-soluble inorganic ions

183 A 100 mg sample was weighed and transferred into a 250 mL bottle. The mixture underwent  
 184 ultrasonic extraction for 20 minutes to ensure complete solubilization. The resulting supernatant  
 185 was then filtered through a 0.45  $\mu\text{m}$  filter for analysis. Based on preliminary experimental results,  
 186 the concentrations of major ions ( $\text{K}^+$ ,  $\text{Na}^+$ ,  $\text{Mg}^{2+}$ , and  $\text{Ca}^{2+}$ ) were measured using Inductively  
 187 Coupled Plasma Optical Emission Spectrometer (ICP-OES, NexIon 2000). Anions ( $\text{Cl}^-$ ,  $\text{SO}_4^{2-}$ , and  
 188  $\text{NO}_3^-$ ) were quantified using ion chromatography (IC). To ensure measurement accuracy, samples  
 189 were organized in sets of twenty, with one randomly selected sample from each group serving as a  
 190 replicate, achieving an error margin of less than 10%. The detection limits for the various  
 191 components were as follows:  $\text{K}^+$  (0.0560 mg/L),  $\text{Na}^+$  (0.0100 mg/L),  $\text{Ca}^{2+}$  (0.0037 mg/L),  $\text{Mg}^{2+}$   
 192 (0.0390 mg/L),  $\text{SO}_4^{2-}$  (0.0090 mg/L),  $\text{NO}_3^-$  (0.0125 mg/L),  $\text{Cl}^-$  (0.0100 mg/L). All standard solutions  
 193 employed in the analysis were sourced from the National Standard Material Center.

194

### 195 **2.3 Trace element analysis**

196 According to the Chinese State Standard “Ambient air and waste gas from stationary sources  
197 emission-determination of metal elements in ambient particles” (HJ 777-2015), the concentrations  
198 of elements such as iron (Fe), aluminum (Al), silicon (Si), titanium (Ti), copper (Cu), cadmium (Cd),  
199 chromium (Cr), manganese (Mn), nickel (Ni), zinc (Zn), lead (Pb), and vanadium (V) were  
200 quantified using Inductively Coupled Plasma Mass Spectrometry (ICP-MS) and ICP-OES. A dust  
201 sample weighing 0.100 g was placed in a Teflon cup, to which 20.0 mL of a nitric acid-hydrochloric  
202 acid digestion solution was added. The sample was heated to reflux at  $100 \pm 5^\circ\text{C}$  for 2 h under a  
203 watch glass, then cooled. Following this, the inner walls of the cup were rinsed with water, and  
204 approximately 10 mL of water was added, allowing the mixture to stand for 30 minutes for  
205 extraction. The extract was then filtered into a 100 mL volumetric flask and diluted to volume with  
206 distilled water for analysis. In cases where organic matter content was high, an appropriate amount  
207 of hydrogen peroxide was introduced during digestion to decompose the organic materials. Prior to  
208 sample analysis, the system was flushed with a rinse solution until the blank intensity value reached  
209 a minimum, and samples were analyzed only after the signal stabilized. If the concentration of any  
210 element exceeded the calibration range, the sample was diluted and reanalyzed.

211

### 212 **2.4 Carbon analysis**

213 This study utilized a combination of wet chemical treatment and thermal/optical reflection  
214 (TOR) to analyze carbon elements in dust deposition (Han et al., 2007b; Han et al., 2007a; Han et  
215 al., 2016). Dust samples were treated with hydrochloric and hydrofluoric acids to remove inorganic  
216 materials. The residual solution was then filtered through a pre-combusted quartz fiber filter  
217 (Whatman, 450 °C for 4 h, diameter 47 mm). This method has been widely applied to measure OC  
218 and EC contents in lake sediments and urban soils (Han et al., 2009; Khan et al., 2009; Han et al.,  
219 2011). Studies have shown that the EC collection efficiency of this method is approximately 99.6%  
220 (Zhan et al., 2013); however, its OC collection efficiency remains unclear. The filtered samples were  
221 air-dried and analyzed for carbon content using a DRI 2001 thermal/optical carbon analyzer  
222 (Atmoslytic Inc., Calabasas, CA) at the Institute of Earth Environment, Chinese Academy of

223 Sciences, adhering to the Interagency Monitoring of Protected Visual Environments (IMPROVE)  
224 protocol.

225 A 0.544 cm<sup>2</sup> disc was extracted from the filter and placed in a quartz boat for analysis. During  
226 the carbon analysis, the samples were initially heated in a 100% helium atmosphere, resulting in the  
227 production of four organic carbon (OC) fractions (OC1, OC2, OC3, and OC4) at four different  
228 temperature levels (140, 280, 480, and 580°C). The atmosphere was subsequently changed to 2%  
229 O<sub>2</sub>/98% He, generating three elemental carbon (EC) fractions (EC1, EC2, and EC3) at three  
230 temperatures (580, 740, and 840 °C). Volatile carbon underwent carbonization in an anaerobic  
231 environment, indicated by a decrease in laser reflectance, and is referred to as pyrolyzed organic  
232 carbon (OPC). In the oxidative atmosphere, OPC was emitted along with the original EC from the  
233 filter. The amount of OPC is defined as the carbon evolved until the laser reflectance returned to its  
234 baseline value (Han et al., 2007b). According to the IMPROVE protocol, EC is calculated as the  
235 total of the three EC subfractions minus OPC (i.e., EC is defined as the sum of EC1, EC2, and EC3,  
236 with OPC subtracted). The method enables differentiation between soot and char, as determined by  
237 the gradual oxidation of these black carbon subtypes in standard reference materials during the EC1  
238 and the EC2 plus EC3 steps, where char is defined as EC1 minus OPC and soot as the sum of EC2  
239 and EC3 (Han et al., 2007a; Han et al., 2016).

240 Please note that in this manuscript, we interchangeably use the terms "EC" and "BC." While  
241 these terms do not strictly refer to the same component, they serve as an adequate approximation  
242 within the scope of this study (Seinfeld et al., 1998; Bond et al., 2004). We use "EC" when discussing  
243 emissions and modeling components, reserving "BC" for climate-related discussions.

244

## 245 **2.5 Statistical analysis**

### 246 (1) Estimation of Secondary Organic Carbon

247 OC consists of primary organic carbon (POC) and secondary organic carbon (SOC). Due to  
248 the intricate physical and chemical processes involved, SOC in urban atmospheres cannot be  
249 directly measured. Therefore, an indirect estimation method, known as the EC tracer method, has  
250 been developed (Turpin and Huntzicker, 1991). If the concentrations of OC and EC are available  
251 and primary OC from non-combustion sources (OC<sub>non-comb</sub>) can be disregarded, EC can be utilized

252 as a tracer for POC from combustion sources, facilitating the estimation of SOC (Turpin and  
253 Huntzicker, 1995):

$$254 \quad \text{POC} = \text{EC} \times (\text{OC}/\text{EC})_{\text{pri}}, \quad (2)$$

$$255 \quad \text{SOC} = \text{OC}_{\text{total}} - \text{POC}, \quad (3)$$

256 where  $\text{OC}_{\text{total}}$  represents total organic carbon.

257 Traditional methods for determining  $(\text{OC}/\text{EC})_{\text{pri}}$  involve regressing OC and EC within a fixed  
258 percentile range of the lowest  $(\text{OC}/\text{EC})$  ratio data (typically 5-20%) or relying on sampling days  
259 characterized by low photochemical activity and local emissions (Castro et al., 1999; Lim and  
260 Turpin, 2002). However, these approaches are limited by their empirical nature, lacking clear  
261 quantitative criteria for selecting the data subsets used to establish  $(\text{OC}/\text{EC})_{\text{pri}}$ . In this study, we  
262 employed the minimum R squared (MRS) method (Millet et al., 2005; Wu and Yu, 2016; Wu et al.,  
263 2018a) to determine  $(\text{OC}/\text{EC})_{\text{pri}}$ . This method calculates a set of hypothetical  $(\text{OC}/\text{EC})_{\text{pri}}$  and SOC  
264 values to identify the minimum correlation coefficient ( $R^2$ ) between SOC and EC, allowing for the  
265 accurate derivation of  $(\text{OC}/\text{EC})_{\text{pri}}$ . The computational procedure followed the algorithm developed  
266 by Wu and Yu (2016) (available at: <https://sites.google.com/site/wuchengust>), implemented within  
267 the Igor Pro environment (WaveMetrics, Inc., Lake Oswego, OR, USA). Due to the limited dataset  
268 size and low temporal resolution, the MRS analysis was performed collectively across all sampling  
269 sites. In this approach, the  $R^2$  between SOC and EC was calculated iteratively for a range of  
270  $(\text{OC}/\text{EC})_{\text{pri}}$  values spanning 0 to 10. The minimum  $R^2$  value of 1.33 (Figure S2) identified the  
271 optimal  $(\text{OC}/\text{EC})_{\text{pri}}$  representative of the true primary ratio.

272

273 (2) Playa salt (ps) and non-playa salt (nps)

274 To differentiate the contributions of salt lake sources to water-soluble ions in atmospheric  
275 deposition, we adopted a methodology similar to that used for marine aerosols. This approach relies  
276 on the ratio of water-soluble ions ( $\text{SO}_4^{2-}$ ,  $\text{Ca}^{2+}$ ,  $\text{K}^+$ ,  $\text{Mg}^{2+}$ ,  $\text{Cl}^-$ ) to  $\text{Na}^+$  in the salt lakes of the QDB,  
277 enabling us to assess the contribution of ps- $\text{Na}^+$  components to nps (Zhang, 1987); details in Zhu  
278 (2025).

$$279 \quad \text{nps-SO}_4^{2-} = [\text{SO}_4^{2-}] - 0.333 \cdot \text{ps-Na}^+, \quad (4)$$

$$280 \quad \text{nps-Ca}^{2+} = [\text{Ca}^{2+}] - 0.062 \cdot \text{ps-Na}^+, \quad (5)$$

$$281 \quad \text{nps-K}^+ = [\text{K}^+] - 0.087 \cdot \text{ps-Na}^+, \quad (6)$$

282 
$$\text{nps-Mg}^{2+} = [\text{Mg}^{2+}] - 0.051 \cdot \text{ps-Na}^+, \quad (7)$$

283 
$$\text{nps-Cl}^- = [\text{Cl}^-] - 2.287 \cdot \text{ps-Na}^+, \quad (8)$$

284 This was accomplished using equations that incorporate total  $\text{Na}^+$ , total  $\text{Ca}^{2+}$ , the average  
 285 crustal ratio  $(\text{Na}^+/\text{Ca}^{2+})_{\text{crust}} = 0.56$  w/w (Bowen, 1979), and the average  $(\text{Ca}^{2+}/\text{Na}^+)$  ratio for Qaidam  
 286 salt lakes,  $(\text{Ca}^{2+}/\text{Na}^+)_{\text{salt lake}} = 0.06$  w/w (Zhang, 1987). Among these, the mass concentration of  
 287  $[\text{SO}_4^{2-}]$ ,  $[\text{Ca}^{2+}]$ ,  $[\text{K}^+]$ ,  $[\text{Mg}^{2+}]$ ,  $[\text{Na}^+]$  and  $[\text{Cl}^-]$  were identified as constituents of dust-fall.

288 
$$\text{ps-Na}^+ = [\text{Na}^+] - \text{nps-Na}^+, \quad (9)$$

289 
$$\text{nps-Na}^+ = \text{nps-Ca}^{2+} \cdot (\text{Na}^+ / \text{Ca}^{2+})_{\text{crust}}, \quad (10)$$

290 
$$\text{nps-Ca}^{2+} = [\text{Ca}^{2+}] - \text{ps-Ca}^{2+}, \quad (11)$$

291 
$$\text{ps-Ca}^{2+} = \text{ps-Na}^+ \cdot (\text{Ca}^{2+} / \text{Na}^+)_{\text{salt lake}}, \quad (12)$$

292

293 (3) HYSPLIT backward trajectory model

294 Backward trajectory clustering analysis was conducted on sampling points using the TrajStat  
 295 plugin within Meteoinfo software. Daily backward trajectories for 48 hours were calculated from  
 296 January 2020 to March 2023 and classified monthly based on differences in the horizontal  
 297 movement direction and velocity of air masses. The trajectories were initiated at Universal Time  
 298 (UTC) 00:00, with a 6-hour increment, originating from 500 m above sea level (Yang et al., 2014).  
 299 Meteorological data utilized in this research were obtained from the Global Data Assimilation  
 300 System (GDAS) provided by the U.S. National Centers for Environmental Prediction (NCEP),  
 301 covering the period from December 2019 to February 2023 (Meteoinfo software website:  
 302 <http://meteothink.org>).

303

304 (4) PMF model

305 PMF is a multivariate factor analysis tool that decomposes a matrix of speciated sample data  
 306 into two matrices: factor contributions (G) and factor profiles (F). The goal of the PMF model is to  
 307 solve the chemical mass balance between measured species concentrations and the respective source  
 308 profiles, with the purpose of minimizing the objective function Q (Eq. 13) based upon the  
 309 uncertainties ( $u_{ij}$ ) of measured species (Paatero and Tapper, 1994).

310 
$$e_{ij} = x_{ij} - \sum_{h=1}^p g_{ih} f_{hj}; Q = \sum_{i=1}^m \sum_{j=1}^n (e_{ij}/h_{ij} s_{ij})^2, \quad (13)$$

311 where  $x_{ij}$  is the measured concentration of the  $j_{th}$  species in the  $i_{th}$  sample at receptor sites.  $f_{kj}$  is the  
312 source profile of the  $j_{th}$  species in the  $k_{th}$  factor and  $g_{ik}$  is the mass contribution of the  $k_{th}$  factor in  
313 the  $i_{th}$  sample.  $e_{ij}$  is the difference between modeled concentrations and measured concentrations.

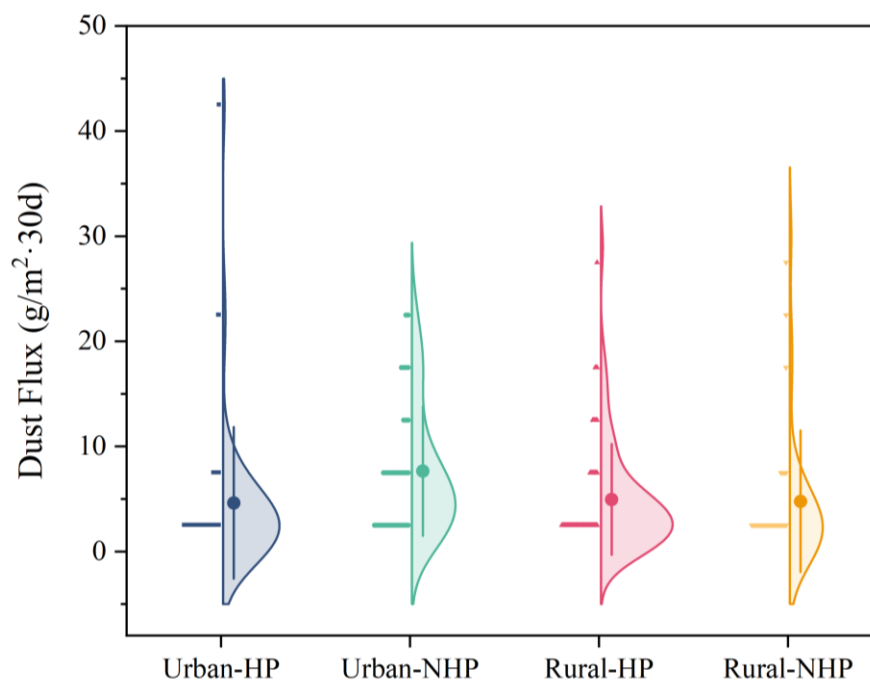
314 The uncertainty for individual species ( $u_{ij}$ ) was defined as the sum of two components: the  $x_{ij}$   
315 multiplied by an error fraction, and one-third of the method detection limit (MDL). For data below  
316 the MDL, concentrations were replaced by 1/2 MDL and the corresponding uncertainty was set to  
317 5/6 MDL (Reff et al., 2007). An extended description of the PMF parameters used in this study and  
318 error estimate based on the model's Q value, displacement (DISP), and bootstrapping (BS) tests  
319 (DISP-BS) are provided in the Supplementary Information. The error assessment and uncertainty  
320 data for the PMF source apportionment can be found in Tables S2 and S3, respectively.

321

### 322 **3. Results and discussion**

#### 323 **3.1 Atmospheric dust deposition flux and water ions concentration**

324 The total deposition flux (DF) in the southern QDB is  $5.41 \pm 5.33 \text{ g/m}^2 \cdot 30\text{d}$ , slightly lower  
325 than that of the Lake Aibi Basin ( $10.77 \text{ g/m}^2 \cdot 30\text{d}$ ) (Li et al., 2022), but higher than the surrounding  
326 areas of Akatama Salt Lake ( $2.93 \text{ g/m}^2 \cdot 30\text{d}$ ) (Wang et al., 2014). Specifically, DF was  $4.67 \pm 4.96$   
327  $\text{g/m}^2 \cdot 30\text{d}$  in rural and  $5.97 \pm 5.73 \text{ g/m}^2 \cdot 30\text{d}$  in urban areas. During the HP, DF in rural and urban  
328 areas were  $4.62 \pm 4.15 \text{ g/m}^2 \cdot 30\text{d}$  and  $4.95 \pm 5.25 \text{ g/m}^2 \cdot 30\text{d}$ , respectively. In contrast, NHP showed  
329 increased DF values of  $4.77 \pm 4.42 \text{ g/m}^2 \cdot 30\text{d}$  (rural) and  $7.66 \pm 6.09 \text{ g/m}^2 \cdot 30\text{d}$  (urban) (Figure 2).  
330 Notably, Urban DF during NHP demonstrated a 54.6% increase relative to HP, while rural DF rose  
331 by 7.1%, contrasting previous findings that associated elevated DF with HP coal combustion (Cheng  
332 et al., 2009; Gao et al., 2013; Guo et al., 2010; Qi et al., 2018). We hypothesize that the increase in  
333 DF during the NHP is attributed to heightened tourism activity (May to September peaks season) in  
334 the QDB (Zhang et al., 2011), attracting approximately 17 million tourists annually, the number  
335 continues to grow. This influx likely leads to increased urban emissions, particularly in densely  
336 populated areas such as DLX and GEM (Figure S3), contributing to the elevated DF levels.



337

338 **Figure 2** Dust flux distribution in urban and rural. The distribution of dust flux in four contexts:

339 Urban with domestic heating period (Urban-HP), Urban with non-HP (Urban-NHP), Rural with

340 domestic heating period (Rural-HP), and Rural with non-HP (Rural-NHP). Each violin plot

341 illustrates the density distribution of dust flux values, with the central dot representing the mean,

342 and the vertical lines indicating the interquartile range.

343

344 Water-soluble ion concentrations differed significantly between rural (115.31 mg/g) and urban

345 (72.81 mg/g) areas. In rural, water-soluble ion content was greater during the HP than in the NHP,

346 while the opposite trend was observed in urban areas (Figure 3 and S4). We categorized the water-

347 soluble ions in dust deposits into ps and nps based on their sources, following the model of marine

348 aerosols (Zhu et al., 2025). Playa salt content consistently surpassed nps in rural areas across both

349 periods, while urban areas showed the opposite trend. Notably, during the NHP, ps content in urban

350 and rural increased by 54.46 and 36.86% respectively. Backward trajectory analysis indicated that

351 airflow in both rural and urban areas primarily originated from the northwest QDB and the eastern

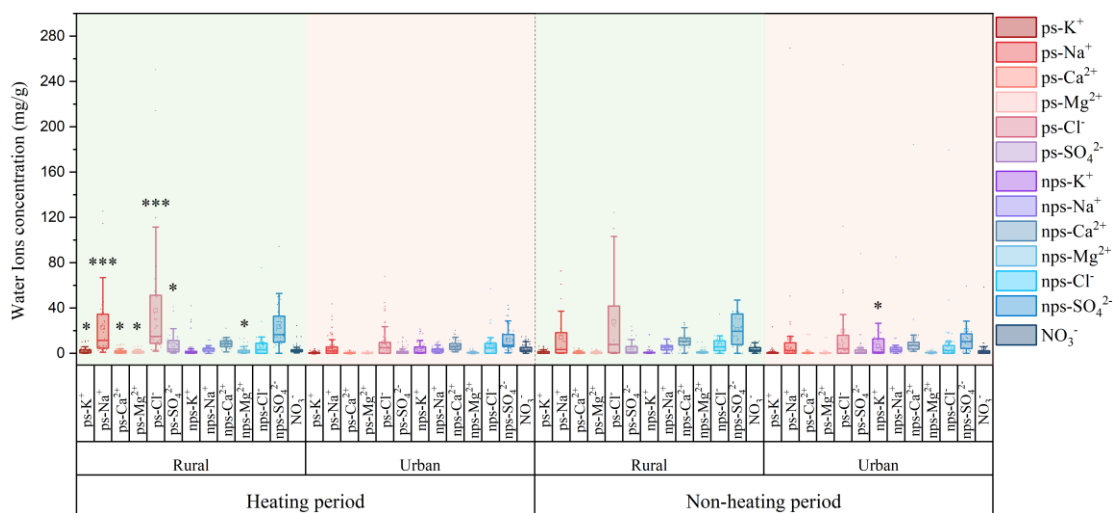
352 Tarim Basin during the HP, while during the NHP, it was influenced more broadly by the salt lake

353 of the QDB (Figure S5 and S6), aligning with the observed variations in ps content. A similar

354 increase in summer sea salt and non-sea salt ions has been reported in Rajkot, India, attributed to

355 ocean wind direction (Gupta and Dhir, 2022).

356 The ratio of  $\text{nps-SO}_4^{2-}/\text{NO}_3^-$  in soluble ions is used to differentiate between coal combustion  
 357 (fixed sources) and vehicular emissions (mobile sources) (Arimoto et al., 1996; Shen et al., 2008).  
 358 The higher  $\text{nps-SO}_4^{2-}/\text{NO}_3^-$  ratio in urban areas compared to rural areas (Figure S7) indicates that  
 359 during the study period, stationary sources (e.g., industrial emissions, coal, and biomass combustion)  
 360 contributed more significantly to the ionic composition of urban dust-fall (Pipal et al., 2019). In  
 361 contrast, the ratio was considerably lower during the NHP than during HP, suggesting that mobile  
 362 sources likely played a more important role in the dust ionic composition during the NHP. Generally,  
 363 emissions from coal combustion and biomass burning was intensified in northern China during the  
 364 HP (Liu et al., 2016), while vehicle emissions dominate during the NHP (Xu et al., 2012), supporting  
 365 the reliability of this analysis. Nevertheless, further investigation integrating atmospheric emission  
 366 inventories, source tracers, aerosol physicochemical processes, and meteorological conditions is  
 367 warranted.  
 368



369  
 370 **Figure 3** Concentrations of water ions in rural and urban across different seasonal periods (domestic  
 371 heating and non-domestic heating periods). Asterisks indicate statistically significant differences  
 372 between sites, with \*,  $P < 0.05$ ; \*\*,  $P < 0.01$ ; \*\*\*,  $P < 0.001$ .

373

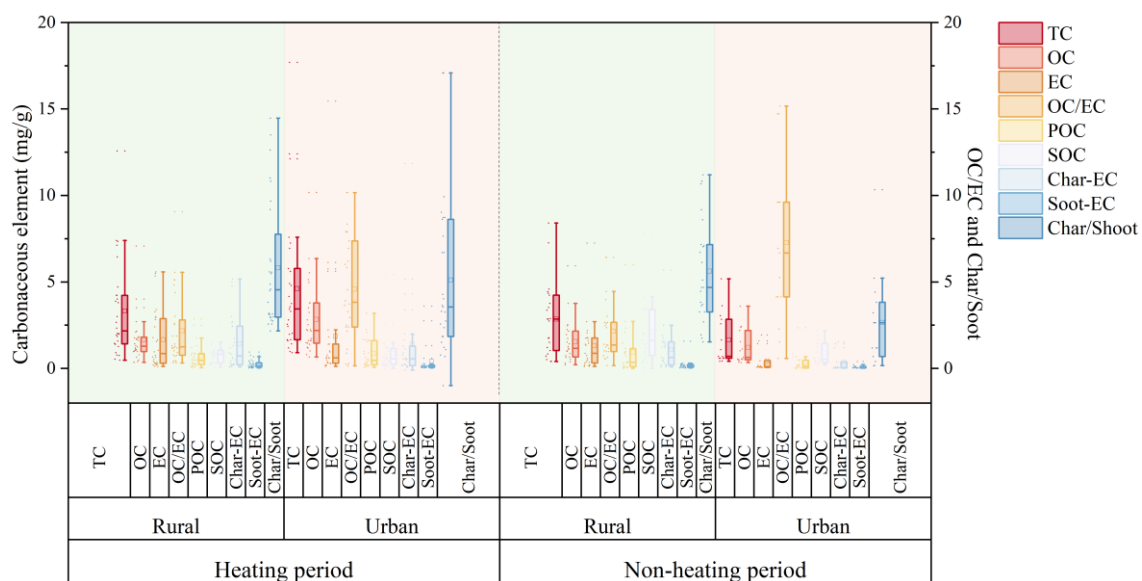
### 374 3.2 Organic carbon and element carbon compositions

375 The average total carbon (TC) concentration in the southern QDB was  $3.83 \pm 3.2$  mg/g,  
 376 significantly lower than that of Huangshi, Hubei province ( $25.15 \pm 11.79$  mg/g) and Washington  
 377 ( $157 \pm 3.2$  mg/g), Kumasi in West Africa (28 mg/g) and Xi'an ( $14.6 \pm 5.8$  mg/g) (Han et al., 2007a;

378 Han et al., 2009b; Zhan et al., 2016; Bandowe et al., 2019), suggesting relatively low carbon  
 379 emissions in the southern QDB. Average OC and EC levels in QDB are markedly lower than those  
 380 in Xi'an (7.4 and 7.2 mg/g, respectively), Wuhu (33.26 and 22.49 mg/g, respectively), and Nanchang  
 381 (25.15 and 11.46 mg/g, respectively) (Han et al., 2009a; Deng et al., 2014; Zhang, 2014), but  
 382 significantly higher, particularly for EC, than in Nam Co (0.35 mg/g) (Chen et al., 2015).

383 In urban, TC content ( $3.05 \pm 2.46$  mg/g) was marginally lower than the rural level ( $3.55 \pm 3.56$   
 384 mg/g), although this difference was not statistically significant. Contrasting spatial patterns emerged  
 385 for carbon components: EC dominated urban areas ( $1.46 \pm 1.60$  mg/g), while OC prevailed in rural  
 386 ( $2.25 \pm 1.92$  mg/g) (Figure 4 and S8). This disparity may be attributed to the long-term combustion  
 387 of biomass, coal, and wood in rural settings (Na et al., 2004). It may also be associated with  
 388 meteorological conditions, particularly heightened solar radiation resulting from reduced primary  
 389 emissions in rural areas, which facilitates the formation of SOC (Xu et al., 2018a; Wang et al., 2019).

390



391

392 **Figure 4** Concentrations of organic carbon (OC), elements carbon (EC), secondary organic carbon  
 393 (OC), primary organic carbon (POC), char-EC, soot-EC and OC/EC, char/soot ratios in different  
 394 sites (Rural, Urban) and seasonal variations (domestic heating and non-domestic heating period).

395

396 Seasonal analysis revealed elevated carbonaceous compound concentrations, specifically OC  
 397 and EC, during the HP. This increase is primarily due to local domestic heating activities coupled  
 398 with adverse meteorological conditions, such as low temperature, weak winds (Oliveira et al., 2007;

399 Gong et al., 2017), weak atmospheric turbulence, and frequent atmospheric inversions (Guo et al.,  
400 2016). Rural emissions primarily stem from coal and biomass burning for heating and cooking  
401 (Zhang et al., 2000; He et al., 2004), contributing to reduced OC and EC content in the NHP, whereas  
402 elevated EC levels in urban areas are primarily linked to vehicular and industrial sources.  
403 Spatiotemporal transport dynamics show EC depletion during rural ward pollutant migration due to  
404 atmospheric dispersion, particularly affecting coarse particulate fractions.

405 Notably, rural carbon emissions exceed urban levels in the southern basin, potentially  
406 attributable to extended HP duration (7 months) compelling low-grade fuel (crop residues, wood,  
407 raw coal and yak dung) utilization (Na et al., 2004). In contrast, urban areas benefit from solar/wind  
408 energy infrastructure and government-led clean heating initiatives (suitable electricity for electricity  
409 policy), achieving 66.63% clean heating penetration (Statistical Yearbook of Haixi Xizang  
410 Autonomous Prefecture of Qinghai Province), leading to a comparatively lower TC content.

411 The OC/EC ratio is a valuable indicator of carbonaceous aerosol sources. In this study, Urban areas  
412 exhibited stable OC/EC ratios ranging from 0.15 to 15.16 (mean = 2.16), whereas rural areas showed  
413 significantly higher ratios during NHP ( $7.27 \pm 4.66$ ) compared to HP ( $4.57 \pm 3.02$ ) (Figure 4 and  
414 S10). Typically, the OC/EC ratio for vehicle emissions ranges from 0.7 to 2.4, for coal combustion  
415 emissions from 0.3 to 7.6, and for biomass burning from 3.8 to 14.5 (Schmidl et al., 2008; Gonçalves  
416 et al., 2010; Pio et al., 2011; Popovicheva et al., 2016).

417 These findings suggest that urban OC/EC ratios (0.15-9.05) are primarily associated with  
418 vehicle and coal combustion, while rural ratios (0.14-15.16) are predominantly linked to coal and  
419 biomass burning. A higher OC/EC ratio typically indicates a greater contribution from biomass  
420 combustion; in this study, the OC/EC ratio of rural was  $5.56 \pm 3.93$ , which is significantly lower  
421 than values recorded in India (8.47) and Nam Co in Xizang ( $16.3 \pm 4.4$ ) (Saud et al., 2013; Chen et  
422 al., 2015), yet higher than those observed in Shanxi (0.7-1.6), Beijing (1.9-2.7), and Tianjin rural  
423 (2.66) (Zhang et al., 2007; Cheng et al., 2015; Wang et al., 2021). This finding indicates that  
424 carbonaceous aerosols in rural QDB derive from both fossil fuel combustion and biomass burning,  
425 suggesting source specificity.

426

### 427 **3.3 Char-EC and Soot-EC compositions**

428 EC is classified into soot and char (Han et al., 2009b), with char-EC and soot-EC defined as  
429 EC1 minus OPC and the sum of EC2 and EC3, respectively (Han et al., 2007). Char-EC is typically  
430 produced from biomass burning at relatively low temperatures, whereas soot-EC originates from  
431 high-temperature coal combustion and automotive emissions (Zhu et al., 2010; Cao et al., 2013).  
432 The char-EC/soot-EC ratio, like the OC/EC ratio, serves as an indicator of carbon aerosol sources.  
433 Since char and soot are mainly generated through combustion processes, their ratio is typically  
434 influenced by two key factors: the primary emission source and the deposition removal efficiency.  
435 For localized PM, such as in urban areas, the removal rate is generally negligible (Han et al., 2009a).

436 Char-EC constitutes 75.88% of rural EC (74.71% HP; 78.84% NHP) and 85.00% of urban EC  
437 (85.58% HP; 84.11% NHP) (Figure 4 and S9), demonstrating its dominance across spatial and  
438 temporal scales. Research suggests that char-EC constitutes a larger proportion of coarse PM, while  
439 soot-EC is more predominant in fine particles, resulting in extended atmospheric residence times  
440 for soot-EC due to reduced deposition velocities (Han et al., 2009b). The increased levels of char-  
441 EC during the urban HP are linked to complex sources, including biomass fuel usage and  
442 transportation emissions, resulting in elevated char concentrations in urban areas and along busy  
443 roadways (Kim et al., 2011).

444 The char/soot ratios for automobile emissions, coal combustion, and biomass burning are 0.60,  
445 1.9, and 11.6, respectively (Chow et al., 2004; Chuang et al., 2014). Generally, high-temperature  
446 combustion (e.g., vehicle and industrial processes) yields lower char and soot concentrations, while  
447 low-temperature combustion (e.g., household cooking and biomass burning) results in higher ratios  
448 (Han et al., 2016; Han et al., 2012; Han et al., 2010; Han et al., 2009a). Differences in char/soot  
449 ratios between urban and rural areas across seasons may be linked to wheat straw burning,  
450 contrasting with minimal vegetation combustion impacts in cities like Xi'an (Cao et al., 2005). The  
451 char/soot ratio for dust-fall observed in this study (4.97; Figure 4 and S10) is slightly higher than  
452 those recorded in Jinchang (3.84) (Han et al., 2009a) and Daheihe, Inner Mongolia (3.2) (Han et al.,  
453 2008). The relatively stable concentration of soot-EC in this study, along with the elevated char/soot  
454 ratio, suggests a correlation with higher coal consumption among local residents and industries. This  
455 indicates that, in comparison to other regions, carbon emissions in the remote QDB are  
456 predominantly sourced from coal and biomass burning, supporting OC/EC ratio findings.  
457 Furthermore, the char/soot ratio is elevated during HP, highlighting the predominant influence of

458 coal and biomass burning in rural areas during HP, while fossil fuel impacts are more pronounced  
459 in NHP.

460

### 461 **3.4 POC and SOC compositions**

462 Aerosol samples with low OC/EC ratios typically exhibit low concentrations of POC, which  
463 mainly comprises primary carbonaceous compounds. The MRS method enables discrimination of  
464 OC into POC and SOC (Method 2.7) (Yoo et al., 2022; Liu et al., 2023). SOC constitutes a dominant  
465 fraction of OC in atmospheric aerosols. Research on carbonaceous aerosols in various Chinese cities  
466 indicates that SOC contributes 67% (53-83%) and 57% (48-62%) to rural and urban OC,  
467 respectively (Zhang et al., 2008)—marginally higher than the 62.62% observed in this study (Figure  
468 4 and S11). Although SOC formation relies on solar radiation, the QDB experiences high levels of  
469 solar energy (Liu et al., 2017), which may facilitate photochemical oxidation of VOCs into SOC  
470 (Hama et al., 2022). Nevertheless, the consistently low SOC concentrations indicate that VOCs  
471 emissions in QDB are significantly lower than the regional averages observed across China,  
472 reflecting relatively low pollution levels. This finding is consistent with the previously observed  
473 low concentrations of atmospheric carbon emission in the region.

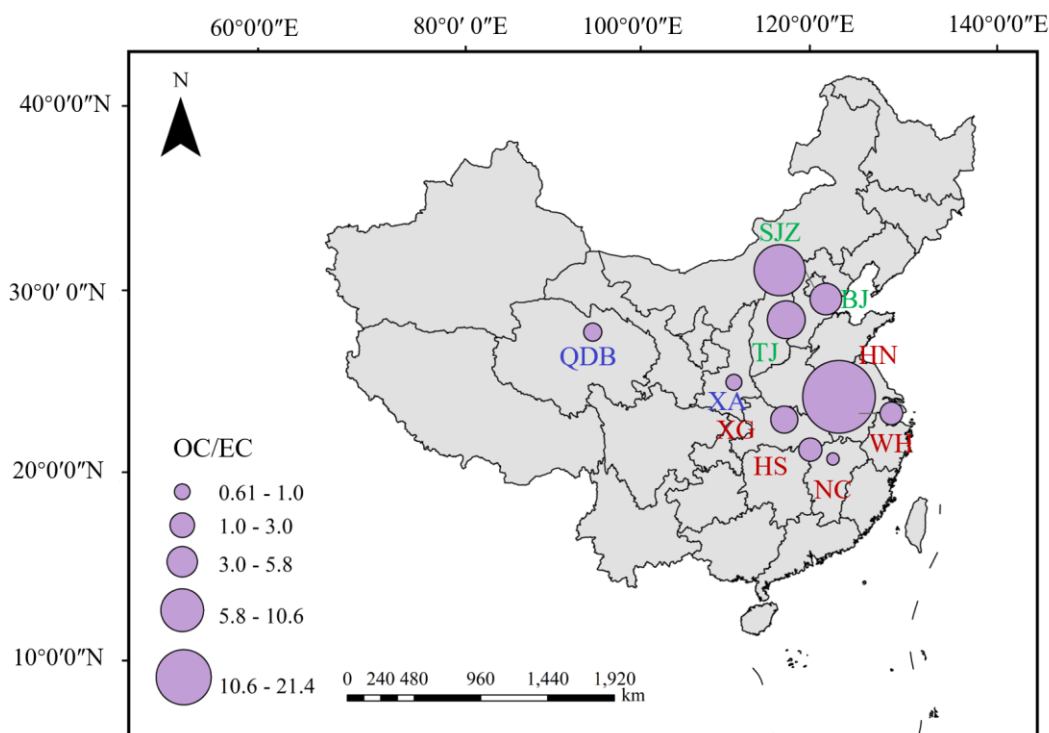
474 During the NHP, rural areas exhibit the highest SOC/OC ratio of 86.70% (Figure S12), while  
475 urban areas record the lowest ratio of 44.32% during the HP. This trend reflects elevated potential  
476 for photochemical activity and reduced contributions from POC, likely due to local emission sources,  
477 such as traffic and coal combustion (Mbengue et al., 2018). The high SOC/OC ratio suggests that  
478 SOC largely displaces OC. Our findings indicate that SOC levels are greater in rural areas (66.52%)  
479 compared to urban regions (58.74%), likely attributable to significant coal consumption for  
480 domestic heating, which enhances emissions of semi-volatile organic compounds and organic gases  
481 (Dan, 2004). As for seasonal variations, studies in California show an increase in SOC levels during  
482 warmer months, which is consistent with our results (Na et al., 2004). This contrasts with the broader  
483 observation that higher temperatures typically lead to lower SOC concentrations (Strader et al., 1999;  
484 Sheehan and Bowman, 2001). This discrepancy may stem from varying sources of SOC emissions  
485 throughout the seasons, necessitating further investigation in conjunction with other carbonaceous  
486 indicators.

487 This study conducted a comparative analysis of carbonaceous element concentrations in  
488 atmospheric dust-fall and road dust between the QDB and other global regions (Table S4). To ensure  
489 data comparability, the selected road dust samples consisted of directly collected in-situ dust without  
490 resuspension treatment. The results revealed that the concentrations of TC, OC, and EC in QDB  
491 (3.27, 1.88, and 1.41 mg/g, respectively) were significantly lower than those in industrial or urban  
492 areas such as Bolu, Turkey; New Delhi, India; and Ezhou, China, and were even lower than many  
493 other Chinese cities (Table S4). The low concentrations of OC and EC in QDB indicate minimal  
494 anthropogenic pollution influence in this region, and the data can represent the regional background  
495 values of carbonaceous components in atmospheric dust-fall in the arid inland areas of East Asia  
496 (Chen et al., 2019a). This is crucial for global models assessing the emission fluxes of carbonaceous  
497 aerosols from dust source regions. In contrast, extremely high values of carbonaceous elements were  
498 found primarily in urban road dust from locations like Bolu, Turkey (TC: 605.2 mg/g), Gwangju,  
499 South Korea (TC: 31.97 mg/g), and Xi'an, China (TC: 36.53 mg/g), indicating strong influences  
500 from traffic emissions (mainly non-exhaust emissions) (Wei et al., 2015; Lee et al., 2018; Demir et  
501 al., 2022). For atmospheric dust-fall in major cities like New Delhi, India, and Wuhan, China, the  
502 carbonaceous components are affected by the combination of traffic emissions (diesel vehicle  
503 emissions being a major source of EC), industrial activities, and emissions from dense populations  
504 (Deng et al., 2014; Zhang, 2014; Zhan et al., 2016; Mishra and Kulshrestha, 2017).

505 The OC/EC ratio in QDB (3.66) is at an intermediate level. It is much lower than that in regions  
506 dominated by biomass burning, such as Kumasi, West Africa (17.07) and Huainan, China (21.4),  
507 but is relatively close to ratios found in cities like Gwangju, South Korea (5.63) and Ulaanbaatar,  
508 Mongolia (5.69), albeit with significantly lower concentrations (Lee et al., 2018; Bandowe et al.,  
509 2019; Liu et al., 2020). We primarily analyzed the OC/EC ratios in cities across different regions of  
510 China to reveal the influence of varying economic development levels.

511 Figure 5 presents spatial variations in urban OC/EC ratios across China. The findings reveal  
512 that the Northwest region, represented by QDB urban and Xi'an (XA) (Han et al., 2009b), exhibits  
513 a significantly lower ratio ( $1.59 \pm 0.56$ ) compared to central regions, including Nanchang (NC)  
514 (Zhang, 2014), Huangshi (HS) (Zhan et al., 2016), Wuhu (WH) (Deng et al. 2014), Xiaogan (XG)  
515 (Zhan et al., 2022), and Huainan (HN) (Liu et al., 2020), where the ratio is  $5.86 \pm 7.81$ . This ratio is  
516 also lower than that observed in eastern cities such as Beijing (BJ) (Tang et al., 2013), Tianjin (TJ)

517 (Ma et al., 2019), and Shijiazhuang (SJZ) (Guo et al., 2018), which have a ratio of  $6.83 \pm 2.77$ . This  
 518 pattern is consistent with the trends in atmospheric PM OC/EC ratios (Xie et al., 2023), suggesting  
 519 that the carbon in the dust of the QDB urban primarily results from coal combustion and industrial  
 520 emissions, leading to elevated EC concentrations and lower OC/EC ratios (Liu et al., 2022).  
 521 Conversely, cities with higher economic development, such as Beijing and Tianjin, characterized by  
 522 greater population density and income levels, typically experience secondary pollution, resulting in  
 523 higher OC/EC ratios. Furthermore, as the pretreatment used in this study removes impurities such  
 524 as silicates from the carbonaceous components of dust, and the OC collection efficiency of this  
 525 treatment is currently unknown, the lower OC/EC ratios observed may also be attributed to a lower  
 526 OC collection efficiency.  
 527



528  
 529 **Figure 5** Distribution of OC/EC ratios across various regions of China. Blue designations  
 530 represent the Northwest region, red indicates the Central region, and green denotes the Eastern  
 531 region. The circle size reflects the magnitude of the OC/EC ratios.

532  
 533 The Char/Soot ratio in QDB is notably high at 5.04, significantly exceeding that of other  
 534 regions such as Xi'an (0.99) and Wuhan (0.09) (Wei et al., 2015; Liu et al., 2021). Char-EC primarily

535 originates from incomplete combustion processes like biomass burning and coal combustion. Soot-  
536 EC mainly derives from high-temperature combustion sources such as fuel oil and diesel vehicle  
537 exhaust (Han et al., 2009). The exceptionally high Char/Soot ratio in QDB strongly indicates that  
538 its limited carbonaceous components predominantly originated from relatively inefficient  
539 combustion sources. These potentially included coal or small-scale biomass burning for local  
540 residential/expedition activities (e.g., heating, cooking) and possibly long-range transported  
541 biomass burning products (e.g., from forest/agricultural fires in South or Southeast Asia) (Han et al.,  
542 2009; Han et al., 2006; Han et al., 2016). In contrast, the very low Char/Soot ratios observed in  
543 cities like Wuhan and Xi'an clearly point to traffic source emissions as their primary contributor, a  
544 finding likely influenced by the specific focus of those studies on road dust.

545         However, we fully recognize the fundamental differences in sources and composition between  
546 road dust and atmospheric dust-fall. Road dust is primarily secondary dust formed from traffic  
547 activities, construction dust, soil particles, and resuspended deposited atmospheric particles, with  
548 its carbonaceous composition strongly reflecting intense local anthropogenic emissions (Casotti  
549 Rienda and Alves, 2021). In contrast, atmospheric dust-fall integrates contributions from local  
550 sources, regional transport, and even long-range transport. Therefore, direct comparison between  
551 these two may introduce bias when interpreting regional pollution characteristics and the degree of  
552 anthropogenic influence, which cannot be overlooked. Building on this analysis, the next phase of  
553 this research will focus on the sampling and analysis of fine atmospheric particulate matter (PM<sub>2.5</sub>  
554 and PM<sub>1</sub>) to more accurately elucidate the emission levels and environmental and climatic impacts  
555 of carbonaceous aerosols in the QDB.

556

### 557 **3.5 Trace elements concentration**

558         The total concentration of major (Fe, Si, Al) and trace elements (Ti, Cr, Cd, Cu, Mn, Ni, Pb, V,  
559 Zn) was determined to be  $8.74 \pm 5.82$  mg/g, while arsenic (As) remained below the detection limit  
560 in all analyzed samples. Crustally derived elements—Fe, Al, Si, and Ti—dominated the elemental  
561 profile, aligning with dust composition patterns reported in Ira, Singapore, and Beijing-Hebei  
562 regions, China (Joshi et al., 2009; Qiao et al., 2013; Eivazzadeh et al., 2021). In comparison to cities  
563 such as Beijing, Shanghai, Xi'an, and Lanzhou, and Junggar Basin the levels of heavy metals in dust

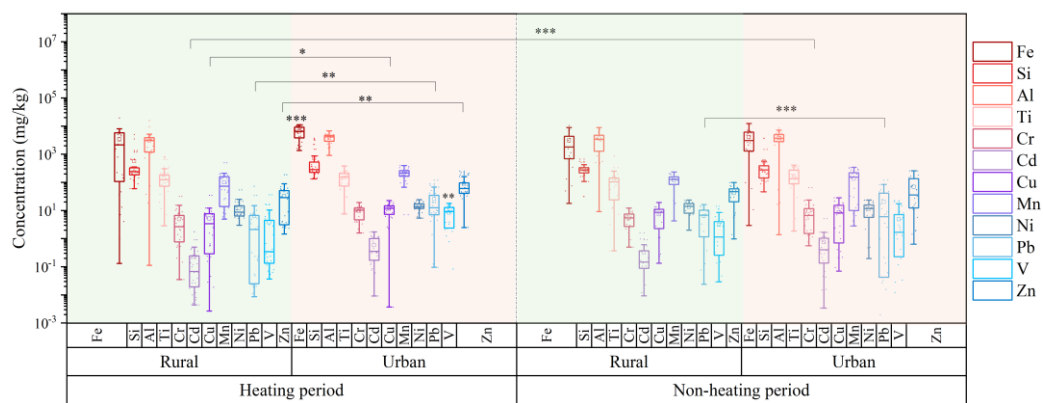
564 from the QDB are relatively low (Jiang et al., 2018) (Supplementary Table S5).

565 The low heavy metal content in dust deposition within the QDB can be attributed to the  
566 following factors. The region has sparse human activity, lacks heavy industrial zones and dense  
567 urban clusters, resulting in low total anthropogenic emissions of heavy metals. Furthermore, the  
568 surface soil in the QDB itself has a low background level of heavy metals, primarily derived from  
569 natural sources with relatively weak influence from human activities (Nuralykyzy et al., 2021; Chen  
570 et al., 2021). From the meteorological perspectives, the basin's high altitude, strong winds, and arid  
571 conditions with minimal precipitation favor the dispersion of atmospheric pollutants. This makes  
572 the formation of prolonged stagnant weather conditions unlikely, thereby preventing the  
573 accumulation of pollutants and the occurrence of high concentrations near the ground. A particularly  
574 unique aspect of the QDB is its role as a significant source of salt dust. The recent study indicates  
575 that salt dust emitted from the playa lakes within the basin contributes substantially to atmospheric  
576 dust deposition (Zhu et al., 2025). These salt dust particles, composed mainly of soluble salts like  
577 NaCl and gypsum, may dilute the relative concentration of non-salt components, such as heavy  
578 metals, when released into the atmosphere in large quantities. The combined effect of these factors  
579 leads to the observed low heavy metal content in dust deposition in this region.

580 Throughout both the HP and NHP, trace elements concentrations in urban areas were  
581 consistently higher than in rural areas, with the exception of Ti (Figure 6 and S13). During the HP,  
582 urban levels of Zn, Pb, and Cu were significantly elevated compared to rural areas, and Pb also  
583 demonstrated a significant increase in urban during the NHP. In rural, the differences in metal  
584 concentrations between HP and NHP were minimal. In contrast, urban areas exhibited higher  
585 concentrations of all elements except for Ti, Cd, and Cr during the HP, with Fe and V showing  
586 notably elevated levels compared to other regions. These variations in average concentrations  
587 indicate that coal combustion for domestic heating in urban areas contributes to increased  
588 atmospheric heavy metal levels (Duan and Tan, 2013; Meng et al., 2017). In contrast, Cd and Cr  
589 exhibited mixed anthropogenic sources with limited coal combustion contributions, while Ti  
590 concentrations remained stable across seasons, reflecting minimal anthropogenic influence.

591 Analysis of the carbonaceous components in QDB dust deposition reveals more intensive coal  
592 combustion in rural areas, yet the heavy metal concentrations in atmospheric deposition are lower  
593 than in urban area. This observation can be explained by the following factors. First, pollution

594 sources in rural areas are relatively singular, whereas urban areas are influenced by more complex  
 595 heavy metal sources. During the heating period, heavy metals in the rural atmosphere of the QDB  
 596 mainly originate from coal and biomass combustion. In contrast, urban areas are affected by a wider  
 597 range of sources, including industrial activities, traffic emissions, and others (Liu et al., 2021; Huang  
 598 et al., 2021a). Additionally, the dense building layout in urban areas hinders pollutant dispersion,  
 599 leading to accumulation, while the open terrain in rural areas facilitates dilution and diffusion. This  
 600 pattern, where rural heavy metal concentrations (particularly Pb, Cr, Cd, As, and other elements  
 601 associated with coal combustion) are lower than those in urban areas during the heating season, has  
 602 also been observed in studies conducted in Northeast China, Shanghai, Taiyuan, the Yangtze River  
 603 Delta, and Southern Nigeria (Shi et al., 2012; Liu et al., 2021; Huang et al., 2021a; Liu et al., 2023b;  
 604 Hilary et al., 2025).  
 605



606  
 607 **Figure 6** Concentration of heavy metals by rural and urban settings during domestic heating and  
 608 non-domestic heating periods. Significant differences are indicated by asterisks (\* $p < 0.05$ ; \*\* $p < 0.01$ ;  
 609 \*\*\* $p < 0.001$ ).

610

### 611 3.6 Source apportionment

612 We conducted a PMF source apportionment analysis on soluble ions, trace and carbonaceous  
 613 elements present in dust, specifically focusing on ps-SO<sub>4</sub><sup>2-</sup>, ps-Ca<sup>2+</sup>, ps-K<sup>+</sup>, ps-Mg<sup>2+</sup>, ps-Cl<sup>-</sup>, ps-Na<sup>+</sup>,  
 614 nps-SO<sub>4</sub><sup>2-</sup>, nps-Ca<sup>2+</sup>, nps-K<sup>+</sup>, nps-Mg<sup>2+</sup>, nps-Cl<sup>-</sup>, nps-Na<sup>+</sup>, Fe, Si, Al, Ti, Cr, Cd, Cu, Mn, Ni, Pb, V,  
 615 Zn, SOC, POC and Char-EC, Soot-EC. Seven source factors were identified based on prior research  
 616 and an understanding of potential local sources: salt lakes, soil, vehicular emissions, secondary  
 617 sources, biomass and coal burning, and industrial activities (Figure 7 and S14). A plot of the time

618 series is provided in Figure S15. The generation of Figure 7a involved extracting factors identified  
619 as the same source from the PMF factor profiles of each site (Urban and Rural) and each heating  
620 season (HP and NHP) shown in Figure S14. The arithmetic mean of the contributions from  
621 characteristic species (elements and ions) corresponding to each factor was calculated. Species with  
622 average contributions exceeding 20% were defined as characteristic species of that source in  
623 atmospheric dust over the QDB.

624 The factor profiles for each element in these source categories represent the arithmetic mean  
625 of profiles from six stations, with detailed operational methods provided in Supplementary Text S1.  
626 The uncertainty of the source contributions was calculated directly from the standard error of the  
627 multiple regression coefficients between the deposition flux (independent variable) and the source  
628 contribution (dependent variable) at different monitoring sites (Belis et al., 2015; Manousakas et al.,  
629 2017). The regression method assumes that all factors explaining the mass have been identified;  
630 however, if a significant portion of the mass not directly related to the species in the PMF analysis  
631 is omitted, the source contributions may be overestimated, which could be an important additional  
632 source of uncertainty. The results are shown in Table S6. It must be noted that this method captures  
633 only a portion of the total uncertainty, as it does not include errors from profile uncertainty or  
634 rotational ambiguity. The low errors calculated by this method indicate a good model fit.

635 The ions  $ss\text{-Na}^+$ ,  $ss\text{-Cl}^-$ ,  $ss\text{-SO}_4^{2-}$ ,  $ss\text{-Ca}^{2+}$ ,  $ss\text{-K}^+$ , and  $ss\text{-Mg}^{2+}$  are widely acknowledged as  
636 indicators of sea salt (Ambade et al., 2022; Aswini et al., 2022; Gluscic et al., 2023). In this study,  
637 we identified  $ps\text{-Cl}^-$  (82.71%),  $ps\text{-Mg}^{2+}$  (79.03%),  $ps\text{-K}^+$  (79.02%),  $ps\text{-Na}^+$  (78.69%),  $ps\text{-Ca}^{2+}$   
638 (78.70%), and  $ps\text{-SO}_4^{2-}$  (78.69%) as key markers of salt lake sources. Furthermore, Cd (29.70%)  
639 was detected at multiple sampling sites, indicating contributions from both salt lakes and industrial  
640 emissions. Salt lake emissions were most pronounced in rural areas during the HP of 2023 at site  
641 LTC and during the NHP of 2020 at site XZH. In urban areas, elevated contributions occurred during  
642 the NHP and HP of 2022 at site GEM, and during the HP of 2023 at site DLX. The contribution of  
643 salt lake sources in rural (12.93%) was significantly higher than in urban (10.33%). During the HP,  
644 the proportion of salt lake sources in rural areas was 5.49%, compared to 20.37% in the NHP; urban  
645 showed contributions of 18.24% during the HP and 2.42% in the NHP, showing opposite seasonal  
646 trends. Backward trajectory simulations indicated that during the HP, air mass in both urban and  
647 rural areas mainly originated from the northwestern part of the basin and the eastern Tarim Basin,

648 whereas during the NHP, they were broadly influenced by the salt lake regions within the basin  
649 (Figure S6). The minor wind direction differences and the inter-distributed sampling points (Figure  
650 1), suggests no substantial geographical disparity between urban and rural sites. Additionally, the  
651 ion content derived from playa salts in dust deposits increased during the NHP in both areas.  
652 Therefore, we propose that the anomalous increase in salt lake contribution during the urban HP  
653 may be closely related to human activities. The enhanced Urban Heat Island (UHI) effect and  
654 temperature inversion structures during the HP can alter boundary layer height, turbulence, and  
655 deposition conditions, thereby increasing the residence time of externally transported particles  
656 within the urban boundary layer and elevating their measured contribution (Cichowicz and  
657 Bochenek, 2024). Urban heat sources and heating emissions may also modify local transport  
658 pathways, leading to more concentrated deposition of dust originating from playa regions over urban  
659 areas. Furthermore, dry road surfaces, increased traffic, and construction activities during the HP  
660 can promote the resuspension of previously deposited playa dust. The use and subsequent  
661 resuspension of road de-icing salts (e.g., NaCl, CaCl<sub>2</sub>) may further amplify the contribution of tracer  
662 ions indicative of playa salts (Gertler et al., 2006; Casotti Rienda and Alves, 2021).

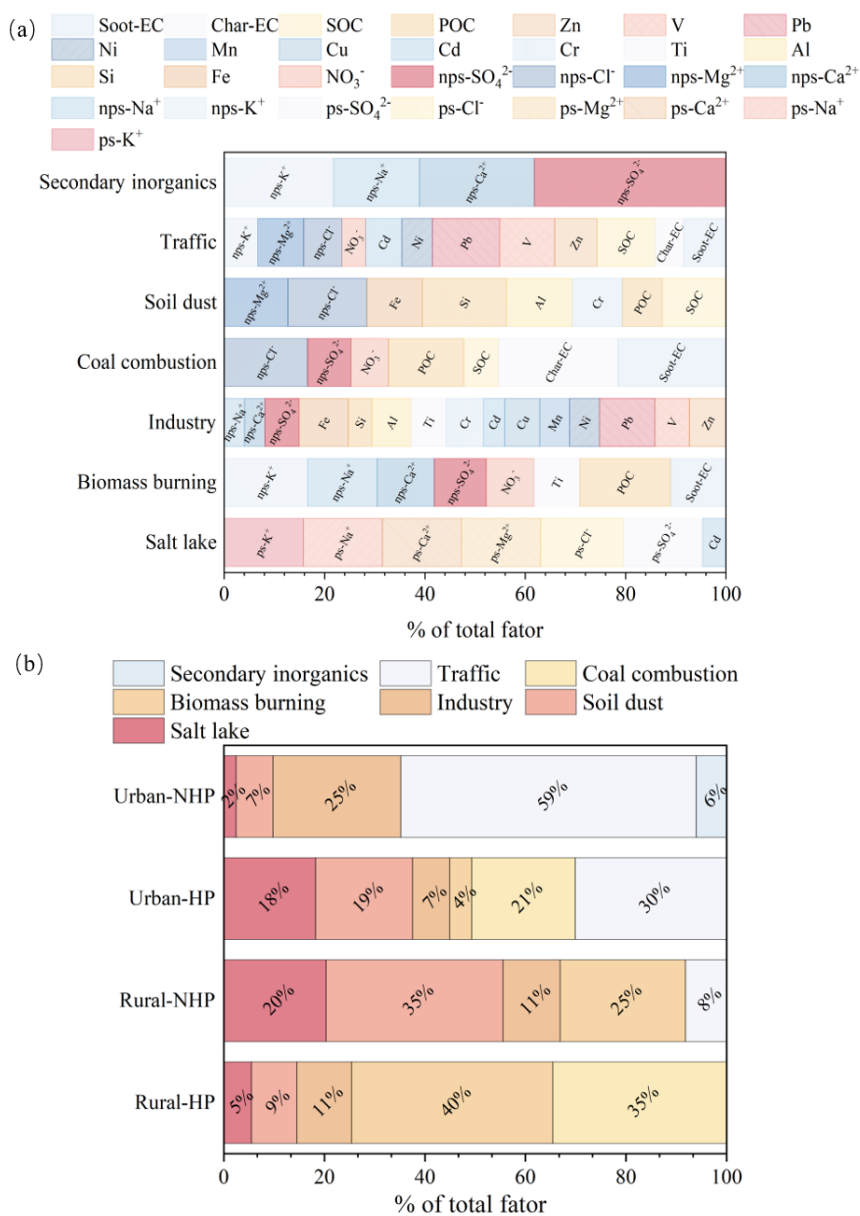
663 The second factor pertains to soil dust, characterized by trace element such as Si (37.17%) and  
664 Al (29.18%), along with ions such as nps-Cl<sup>-</sup> (34.90%), nps-Mg<sup>2+</sup> (28.21%), and Fe (24.43%)  
665 (Pervez et al., 2018; Tian et al., 2021). Additionally, the proportions of elements such as SOC  
666 (28.20%) and POC (17.70%) suggest that the dust is likely mixed with fossil fuel emissions. Mg,  
667 Al, Si, and Fe are typical tracers for soil dust (Liu et al., 2003; Heo et al., 2009). The temporal  
668 variation of soil dust was largely consistent with that of the salt lake source, indicating the fact that  
669 they may be influenced by similar factors. Notably, the contribution of soil dust in rural areas  
670 (22.11%) exceeded that in urban areas (13.33%), indicating that soil dust is a major source of  
671 atmospheric deposition. In urban areas, the contribution during the NHP was relatively low (7.36%),  
672 likely due to higher wind speeds and the effectiveness of frequent summer precipitation (Zhang et  
673 al., 2015a).

674 The third factor is traffic emissions, which are particularly pronounced in urban areas. Key  
675 characteristic elements include Pb (59.52%), V (48.73%), nps-Mg<sup>2+</sup> (40.78%), Zn (37.47%), nps-  
676 Cl<sup>-</sup>(33.83%), Cd (32.43%), nps-K<sup>+</sup>(29.64%), Ni (27.01%), NO<sub>3</sub><sup>-</sup> (20.99%)and SOC (51.71%), Soot-  
677 EC (37.56%), Char-EC (24.94%) (Adeniran et al., 2017). In rural areas, vehicular emissions

678 contributed 8.17% to atmospheric deposition during the NHP, whereas in urban areas, the  
679 contribution was significantly higher at 45.13%, with 30.07% during the HP and 58.78% in the NHP.  
680 These findings correlate with previous studies on OC/EC and char/soot ratios, suggesting that  
681 carbonaceous elements in the NHP primarily derive from vehicular emissions. The traffic emission  
682 factor in the QDB represents a mixture of vehicle exhaust and non-exhaust sources (e.g., tire and  
683 brake wear, and resuspended road dust). Elements and ions including V, NO<sub>3</sub><sup>-</sup>, Ni, and carbonaceous  
684 components primarily associated with vehicle exhaust (Cong et al., 2011; Zhang et al., 2012). For  
685 instance, Ni can be emitted from fuel combustion and vehicle exhaust (Pacyna and Pacyna, 2001).  
686 In contrast, elements such as Cu, Zn, nps-Mg<sup>2+</sup>, and nps-K<sup>+</sup> originate from non-exhaust vehicle  
687 emissions, including brake and tire wear, as well as the resuspension of road dust (Amato et al.,  
688 2014). For example, Zn may derive from the wear of rubber tires on roads (Rogge et al., 1993), Pb  
689 emissions may be related to wear (tires/brakes) (Smichowski et al., 2007), and Cu is associated with  
690 brake wear (Lin et al., 2015). Furthermore, the presence of crustal elements and ions such as Fe, Si,  
691 and nps-Mg<sup>2+</sup> in the traffic emission factor for Urban-NHP, Urban-HP, and Rural-NHP suggests an  
692 additional contribution from resuspended road dust (Chen et al., 2019). For traffic emissions during  
693 the NHP, peaks were observed in both rural and urban areas in 2022, generally concentrated in July,  
694 August, and September, coinciding with the tourism high season. During the HP, traffic emissions  
695 primarily occurred in 2021 at GEM and in 2023 at DLX. Due to the impact of the COVID-19  
696 pandemic, tourist numbers in the QDB sharply declined in 2020 and 2021. The peak in tourism  
697 activity in 2022 (Qinghai Statistical Yearbook, 2022) corresponded with the highest level of traffic  
698 emissions during the three-year period, indicating a direct impact of tourism flux on emission levels.  
699 However, given the relatively short sampling duration of this study (three years), longer-term data  
700 and further research are needed to substantiate this hypothesis.

701 The fourth factor is coal combustion, characterized by high concentrations of nps-Cl<sup>-</sup> (50.93%),  
702 nps-SO<sub>4</sub><sup>2-</sup> (26.61%), NO<sub>3</sub><sup>-</sup> (22.82%), and Char-EC (73.01%), Soot-EC (65.98%), POC (46.04%),  
703 SOC (21.12%) (Kundu and Stone, 2014; Contini et al., 2016). Zhang et al (2023) found that coal  
704 combustion emits particles rich in Cl<sup>-</sup>. Coal combustion was more intense at site LTC in rural areas  
705 and at site DLX in urban areas. Coal combustion occurs exclusively during the HP, contributing  
706 34.57% in rural areas and 20.63% in urban areas. These results align with earlier studies on  
707 carbonaceous aerosols, indicating that the carbon content from coal combustion emissions is higher

708 in rural regions than in urban environments. Consistent with northern China, air pollution in QDB  
 709 urban has declined due to the adoption of clean heating technologies (Zhang et al., 2021; Xue et al.,  
 710 2023). However, rural coal combustion remains a major source of carbonaceous aerosols during the  
 711 HP.  
 712



713  
 714 **Figure 7** Factor profile and contributions in urban and rural area. (a) presents the factor profiles,  
 715 represented as the arithmetic mean of individual elements across various locations, highlighting  
 716 only those elements that constitute more than 20% of each profile. (b) illustrates the contributions  
 717 of different sources at each location. [HP, domestic heating period; NHP, non-domestic heating  
 718 period].

719 The fifth factor, biomass burning, is characterized by significant concentrations of non-  
720 precipitating species, including nps-K<sup>+</sup> (42.76%), nps-Na<sup>+</sup> (35.49%), nps-Ca<sup>2+</sup> (29.23%), nps-SO<sub>4</sub><sup>2-</sup>  
721 (26.56%), NO<sub>3</sub><sup>-</sup> (24.46%), Ti (23.41%) and POC (46.48%), Soot-EC (28.33%) (Simoneit, 2002;  
722 Sulong et al., 2019). K<sup>+</sup> serves as an important tracer for biomass burning (Cachier and Ducret,  
723 1991). Biomass burning contributes 32.82% to rural atmospheric dust deposition, with a higher  
724 proportion during the HP (39.21%) compared to NHP (26.44%). Biomass burning made significant  
725 contributions in urban areas in 2021 and 2022. In rural areas, biomass burning emissions were  
726 particularly strong, especially during the HP at LTC and the NHP at XZH. In urban, biomass burning  
727 is primarily observed during the HP, contributing only 2.19%. These findings underscore biomass  
728 burning as a major source of carbon emissions in rural settings, aligning with the prevalent use of  
729 biomass fuels for cooking and domestic heating in Northern China's rural areas (Meng et al., 2019),  
730 where 70% to 80% of energy demand are fulfilled by materials such as dung cakes, firewood,  
731 charcoal, and crop residues (Tao et al., 2018; Shi et al., 2019). Furthermore, increased biomass  
732 burning is also associated with the autumn harvest period (Chen et al., 2017; Li et al., 2021).

733 The sixth factor pertains to industrial emissions, which are characterized by high  
734 concentrations of Pb (55.18%), Fe (48.91%), Cr (37.05%), Zn (36.42%), Ti (35.10%), Cu (34.91%),  
735 V (34.44%), Ni (29.69%), Mn (29.59%) and Cd (21.29%) (Almeida et al., 2015; Yao et al., 2016).  
736 These elements were consistently detected across all sampling sites, alongside Al (38.84%), nps-  
737 SO<sub>4</sub><sup>2-</sup> (34.15%), Si (23.39%) and nps-Ca<sup>2+</sup> (20.48%), nps-Na<sup>+</sup> (20.02%), which indicate potential  
738 contributions from soil dust. Zn, Cu, Fe, and Mn are major chemical components in industrial  
739 emission profiles; Cd is a trace element found in metallurgical industries (Xu et al., 2022), while Zn  
740 and Mn emitte from oil combustion, metallurgy, and steel manufacturing processes (You et al., 2017).  
741 Pb and Cd are associated with metal smelting and processing (Fang et al., 2021). Industrial  
742 emissions showed greater contributions during the HP at XZH and at DLX. In rural areas, industrial  
743 emissions constitute 11.10% of carbon output, with contributions of 10.86% during the HP and  
744 11.33% during the NHP. In urban areas, industrial emissions account for 16.41% overall, with 7.37%  
745 during the HP and 25.44% in the NHP. Due to the abundance of non-ferrous metal resources (e.g.,  
746 lead-zinc ores), oil, natural gas, and saline minerals (e.g., potassium, lithium) in the QDB, the  
747 primary industrial activities are mining and associated chemical industries. Particularly around the  
748 GEM and DLX sites, the presence of numerous lead-zinc, iron, and copper mining enterprises leads

749 to significant contributions from industrial emissions to urban dust fallout, making it one of the  
750 major sources of air pollution in the basin.

751 The seventh factor is secondary inorganic aerosols, primarily composed of  $\text{NO}_3^-$  (68.54%), nps-  
752  $\text{Mg}^{2+}$  (41.04%), nps- $\text{Na}^+$  (39.01%) and nps- $\text{Ca}^{2+}$  (30.79%) (Liu et al., 2015; Liu et al., 2016a). High  
753 mass loadings of  $\text{NO}_3^-$  and  $\text{SO}_4^{2-}$  are characteristic of typical secondary inorganic aerosols (Huang  
754 et al., 2021). Research indicates that  $\text{NO}_3^-$  and  $\text{SO}_4^{2-}$  primarily result from the conversion of gaseous  
755 precursors, such as  $\text{SO}_2$  and  $\text{NO}_x$ , through photochemical reactions, predominantly sourced from  
756 local and regional emission (Liu et al., 2015; Tao et al., 2013). Secondary inorganic aerosols are  
757 predominantly observed in urban areas during the NHP, where they contribute 6.00% to total aerosol  
758 sources. This increase is likely due to elevated temperatures and enhanced solar radiation during  
759 this period, which promote photochemical activity (Pandolfi et al., 2010). The secondary inorganic  
760 aerosol source was identified only in Urban-NHP, peaking in August 2022 at GEM and in June, July,  
761 and August 2022 at NMH. This trend closely followed the distribution of traffic emissions,  
762 suggesting that the formation of secondary aerosols is linked to increased traffic activity. Traffic  
763 emissions, particularly vehicle exhaust, are a significant source of secondary inorganic aerosols  
764 (especially  $\text{NO}_3^-$ ) in urban atmospheres (Ma et al., 2017). Source apportionment studies in Beijing  
765 have similarly found that the contribution of secondary inorganic aerosols increases in summer,  
766 closely associated with traffic emissions (Zhang et al., 2013).

767 Dust deposition sources exhibit significant seasonal and spatial variations. In the QDB, coal  
768 combustion (27.60%) and biomass burning (22.21%) dominate during HP, transitioning to traffic  
769 emissions (33.48%), soil dust (21.27%) and industry emission (18.39%) as the primary contributor  
770 in NHP. Rural areas predominantly contribute to dust through biomass burning and coal combustion,  
771 as well as natural sources like windblown dust and salt lake emissions. This pattern aligns with  
772 increased coal usage for winter domestic heating and heightened biomass burning for cooking and  
773 heating in rural areas. In urban, dust deposition is briefly influenced by anthropogenic activities,  
774 including traffic and industrial emissions, with minimal contributions from domestic heating. Such  
775 differences can be attributed to varying economic development models, industrial and energy  
776 structures, and levels of human activity (Kataki et al., 2016).

777 This study observed that the contribution of biomass burning to atmospheric dust deposition in  
778 rural areas of the QDB during the HP was higher than that of soil dust. Given that the collected dust

779 samples had particle sizes  $>10\ \mu\text{m}$ , while biomass burning typically emits aerosols in the submicron  
780 range, we propose several potential explanations. Firstly, during the HP, factors such as increased  
781 soil moisture and snow cover significantly suppress soil dust emission, resulting in a lower intensity  
782 than in other seasons (An et al., 2018; Yang et al., 2019). Simultaneously, biomass and coal burning  
783 for heating increases substantially, leading to intense, short-term emissions of fine particles.  
784 Although it was fine initially, these high-concentration ultrafine particles can undergo coagulation  
785 or coalescence, aggregating with each other or onto pre-existing coarse particles, thereby increasing  
786 their size (Butler and Mulholland, 2004; Kulmala et al., 2004; Li et al., 2020). Furthermore, fine  
787 particles from biomass burning (e.g., carbonaceous materials) may mix internally with coarse  
788 particles like soil dust or salt dust from the QDB, forming internally mixed particles (Li et al., 2003;  
789 Hand et al., 2010). During source apportionment, such coarse particles are more likely to be  
790 attributed to the biomass burning source. Additionally, the QDB is a significant source of salt dust  
791 (Zhu et al., 2025). Salt dust particles (e.g., halite, gypsum) provide excellent condensation nuclei  
792 for soluble substances emitted from biomass burning, greatly promoting hygroscopic growth (Li et  
793 al., 2003; Kumar, 2010; Wang, 2013). The basin's topography also favors stable inversion layers,  
794 inhibiting pollutant dispersion and allowing particles more time to grow, mix, and age in the  
795 atmosphere. Prevailing wintertime winds may also transport pollutants from surrounding regions  
796 into the basin.

797 Moreover, the dust in this study was collected using a passive sampler. Over 90% of the  
798 collected dust particles were smaller than  $100\ \mu\text{m}$ , with approximately 25% less than  $10\ \mu\text{m}$  (Figure  
799 S16), indicating the presence of fine particles ( $<10\ \mu\text{m}$ ), albeit in a relatively small proportion. The  
800 particle size distribution of atmospheric dust deposition is similar to that of TSP, with both primarily  
801 consisting of particles smaller than  $100\ \mu\text{m}$ . Using PMF source apportionment, this study identified  
802 a notably high contribution from biomass burning in rural areas, particularly during the heating  
803 period. Similarly, studies on atmospheric TSP in Iran (Ashrafi et al., 2018), the Qinghai-Xizang  
804 Plateau (Lulang) (Zhao et al., 2013), Northeast China (Jia et al., 2024), and Qingdao (Liu et al.,  
805 2022) have also reported significant contributions from biomass and coal combustion. This suggests  
806 that contributions from biomass and coal combustion can indeed be observed in particles larger than  
807  $10\ \mu\text{m}$ . Finally, the PMF model may have uncertainties in resolving sources with similar chemical  
808 profiles. If the chemical compositions of local soil dust and biomass burning particles overlap after

809 long-range transport and complex atmospheric reactions, the model might not fully separate them  
810 (Cesari et al., 2016).

811

### 812 **3.7 Environmental implication**

813 The source apportionment analysis using the PMF model indicates that in the QDB, rural dust-  
814 fall predominantly originates from the combustion of solid fuels, including firewood, yak dung, and  
815 coal, accounting for approximately 74.61% of the total contribution. This proportion significantly  
816 exceeds contributions reported for rural areas in Beijing (41%) (Hua et al., 2018), Agra (54.3%)  
817 (Agarwal et al., 2020), and Beihai, Guangxi Province (66.7%) (Zhang et al., 2019).

818 The higher contribution in this study likely reflects the local energy profile, as the sampling  
819 site in Haixi Mongol and Xizang Autonomous Prefecture, Qinghai Province, primarily relies on coal,  
820 yak dung, and firewood, constituting 58%, 23.5%, and 13% of rural energy consumption,  
821 respectively (Jiang et al., 2020; Shen et al., 2021). In contrast, solid biomass fuels, including wood  
822 and yak dung, account for over 70% of rural household energy consumption in Xizang, with yak  
823 dung alone representing 53% (Liu et al., 2008; Xiao et al., 2015). Similar patterns emerge in South  
824 and Central Asia, where biomass fuels dominate residential heating (firewood: 39%; dung: 29%)  
825 (Amacher et al., 1999; Heltberg et al., 2000; Hoeck et al., 2007; Foysal et al., 2012; Behera et al.,  
826 2015; Kerimray et al., 2018). In northern China, rural domestic heating primarily relies on coal  
827 (46%), firewood (23.8%), and electricity (15.1%) (Tao et al., 2018), further highlighting the unique  
828 energy composition of QDB.

829 Recent studies have shown that South Asia, Central Asia, and Xizang contribute significantly  
830 to high concentrations of atmospheric PM, particularly BC, which accelerates glacier melting in the  
831 QXP (Ming et al., 2010; Xia et al., 2011; Chen et al., 2015). The QDB is recognized as a significant  
832 dust source affecting the glacier surfaces on the QXP, although it is often overlooked (Dong et al.,  
833 2014; Wei et al., 2017; Zheng et al., 2021). Compared to other dust sources, the QDB exhibits higher  
834 emissions from coal combustion, giving it a unique influence on the QXP. The organic matter and  
835 pollutants, such as polycyclic aromatic hydrocarbons (PAHs), released from household solid fuel  
836 combustion, particularly coal (98%) and dung (94%), are substantially higher than those from  
837 firewood (Leavey et al., 2017; Secrest et al., 2017; Ye et al., 2020). Consequently, the impact of PM

838 from coal combustion in the QDB on the QXP is significant. Specifically, the presence of BC in PM  
839 increases glacier albedo, accelerating the melting of glaciers and snow in the region (Kang et al.,  
840 2020) and impacting global freshwater resources (Huss and Hock, 2018). Additionally, BC enhances  
841 cloud condensation nuclei (CCN), ice number concentration, and cloud cover (Zhou et al., 2025),  
842 thereby influencing global climate change. Furthermore, coal combustion releases harmful  
843 emissions, including CO<sub>2</sub>, NO<sub>x</sub>, CO, SO<sub>2</sub> and sulfur trioxide (SO<sub>3</sub>) (Munawer, 2018), adversely  
844 affecting local human health and exacerbating climate warming on the QXP (Liu et al., 2006; Li et  
845 al., 2023), with broader implications for global climate. Therefore, the atmospheric pollutants  
846 emission of the QDB deserves considerable attention. However, this study focuses primarily on  
847 larger particles, indicating a need for further research on the environmental impacts of carbonaceous  
848 aerosols in atmospheric PM within the QDB.

849 In addition to the distinctive energy consumption structure in the rural QDB, which leads to  
850 significant contributions from coal and biomass burning during HP, atmospheric dust deposition in  
851 the QDB during the NHP primarily originates from traffic and industrial emissions. The contribution  
852 from traffic emissions during the NHP was twice that during the HP. Considering the larger particle  
853 size of the dust samples collected in this study, the traffic-related dust is likely derived mainly from  
854 vehicle non-exhaust emissions, such as road dust (Gondwal and Mandal, 2021). This indicates that  
855 NHP atmospheric conditions are significantly influenced by resource development and tourism.  
856 Sampling sites, such as Qarhan Salt Lake, along with GEM and LTC stations within approximately  
857 100 km (Figure 1), suggest that salt lake resource extraction has a lower impact on regional aerosols  
858 than traffic emissions, despite salt lakes being the primary resource. This is likely because salt lake  
859 development mainly involves solar evaporation and chemical processes like extraction and  
860 adsorption, which emit fewer pollutants compared to other mining methods (Zhen, 2010).  
861 Consequently, salt lake resource exploitation exerts a relatively minor effect on local atmospheric  
862 carbonaceous aerosol.

863 Similar salt lakes with comparable environments to QDB, such as Salar de Uyuni in Bolivia,  
864 the Atacama Salt Lake in Chile, and Ombre Muerto in Argentina, are rich in lithium resources (Li  
865 et al., 2014), making them focal points for resource development. Additionally, Salar de Uyuni, the  
866 Atacama Salt Lake, Junggar Basin, and the Great Salt Lake are renowned tourist destinations. This  
867 suggests that, in arid basin salt lakes with similar climates and intensive human activity, atmospheric

868 carbonaceous aerosols are likely influenced by resource exploitation and tourism, especially tourism.  
869 The study's findings can inform policy decisions regarding unexploited salt lakes in South America,  
870 such as Ombre Muerto and Salar de Uyuni. However, while QDB also hosts mineral resources such  
871 as copper, iron, and tin, this research focused on larger particles ( $>100\ \mu\text{m}$ ), which are more  
872 indicative of local sources. Given that sampling was conducted around the salt lakes, potential  
873 impacts from other mineral resource developments may have been underestimated. Further research  
874 is necessary to fully assess the environmental effects of carbonaceous aerosols in QDB atmospheric  
875 particles.

876

## 877 **Conclusion**

878 This study analyzed the composition of dust deposition at six sampling sites in the southern  
879 Qaidam Basin from January 2020 to March 2023 and examined DF, soluble ions, trace and  
880 carbonaceous element content in urban and rural samples during both domestic heating and non-  
881 domestic heating periods. Through integrated application of backward trajectory modeling, PMF,  
882 and carbon speciation indices, we identified dominant dust sources and evaluated domestic heating  
883 impacts on atmospheric processes in remote regions.

884 The findings revealed that DF and carbon emissions were significantly higher in rural than in  
885 urban areas. Among carbon indicators, urban areas exhibited elevated EC levels ( $1.46 \pm 1.60\ \text{mg/g}$ ),  
886 while OC levels were higher in rural ( $2.25 \pm 1.92\ \text{mg/g}$ ). Economic development increase OC/EC  
887 ratios, but they are driven by different intrinsic factors. Char-EC was the dominant contributor to  
888 EC (80.44%), with urban Char-EC levels (85.00%) showing a notable increase compared to rural  
889 levels (75.88%). SOC was the principal contributor to OC (68.17%), with rural SOC levels  
890 surpassing (67%) those in urban areas (57%). The OC/EC and char-EC/soot-EC ratios, along with  
891 PMF results, indicated that during HP, dust deposition in the QDB was primarily derived from coal  
892 combustion (28.44%) and biomass burning (22.14%), while traffic emissions accounted for 34.19%  
893 of dust during NHP. Coal and biomass burning were the main contributors to rural dust, strongly  
894 influenced by domestic heating, whereas urban dust predominantly originated from traffic (45.13%)  
895 and industrial emissions (16.41%). Compared to other dust sources in the Qinghai-Xizang Plateau,  
896 coal consumption in the QDB is higher during the domestic heating period. The resulting emissions

897 of black carbon and greenhouse gases may exacerbate glacier melting in the region, warranting  
898 increased attention. Given the distinctive carbonaceous aerosol signatures identified in the Qaidam  
899 Basin, we recommend prioritizing their radiative forcing effects in regional environmental  
900 policymaking and climate modeling frameworks. Furthermore, findings of this study offer a  
901 valuable scientific basis for understanding atmospheric carbonaceous aerosols in arid basins and  
902 salt lake regions with climates similar to QDB. They can particularly inform policy decisions  
903 regarding unexploited salt lakes in South America, such as Ombre Muerto and Salar de Uyuni.

904 However, this study primarily focused on larger-scale PM and examined the effects of heating  
905 on carbonaceous aerosols in the QDB. It lacks an investigation of aerosols with smaller particle  
906 sizes (e.g., PM<sub>10</sub>, PM<sub>2.5</sub>, PM<sub>1</sub>), which is essential for a comprehensive understanding of  
907 carbonaceous aerosol characteristics in this unique region. Furthermore, in addition to offline  
908 observations, future research should incorporate online observations with high spatiotemporal  
909 resolution and utilize numerical air quality models such as CMAQ, CAMx, WRF-CHEM, and  
910 NAQPMS to analyze the spatiotemporal distribution and future trends of carbon aerosols in the  
911 QDB.

912

### 913 **Author contribution**

914 HZ: Conceptualization, data curation, formal analysis, funding acquisition, investigation,  
915 methodology, project administration, validation, writing – original draft.

916 LZ: Data curation, formal analysis, methodology.

917 SZ: funding acquisition, validation, writing – review & edited.

918 XZ: Supervision, conceptualization, funding acquisition, writing – review & edited.

919

### 920 **Acknowledgements**

921 This research was funded by Youth Joint Fund of Lanzhou Branch of Chinese Academy of Sciences  
922 (E4400304), and by Qinghai Provincial Innovation Platform Construction Special Program (Project  
923 No. 2024-ZJ-J03), and supported by Qinghai Provincial Key Laboratory of Geology and  
924 Environment of Salt Lakes (No. The Science and Technology Plan Project of Qinghai Province  
925 Incentive Fund 2024).

926

927 **Declaration of competing interest**

928 The authors declare that there is no conflict of interest.

929

930 **Data availability**

931 Datasets for this research has been uploaded in Zenodo and is available at

932 <https://doi.org/10.5281/zenodo.14382853> (Zhu, 2024).

933 **Reference**

- 934 Abdollahi, S., Karimi, A., Madadi, M., Eslamian, S., Ostad-Ali-Askari, K., and Singh, V. P.: Lead  
935 concentration in dust fall in Zahedan, Sistan and Baluchistan Province, Iran, *Journal of Geography*  
936 and *Cartography*, 4, 6, 10.24294/jgc.v4i2.601, 2021.
- 937 Adeniran, J. A., Yusuf, R. O., and Olajire, A. A.: Exposure to coarse and fine particulate matter at and  
938 around major intra-urban traffic intersections of Ilorin metropolis, Nigeria, *Atmospheric*  
939 *Environment*, 166, 383-392, 10.1016/j.atmosenv.2017.07.041, 2017.
- 940 Agarwal, A., Satsangi, A., Lakhani, A., and Kumari, K. M.: Seasonal and spatial variability of secondary  
941 inorganic aerosols in PM<sub>2.5</sub> at Agra: Source apportionment through receptor models, *Chemosphere*,  
942 242, 125132, <https://doi.org/10.1016/j.chemosphere.2019.125132>, 2020.
- 943 Aiken, A. C., DeCarlo, P. F., Kroll, J. H., Worsnop, D. R., Huffman, J. A., Docherty, K. S., Ulbrich, I. M.,  
944 Mohr, C., Kimmel, J. R., Sueper, D., Sun, Y., Zhang, Q., Trimborn, A., Northway, M., Ziemann, P.  
945 J., Canagaratna, M. R., Onasch, T. B., Alfarra, M. R., Prevot, A. S. H., Dommen, J., Duplissy, J.,  
946 Metzger, A., Baltensperger, U., and Jimenez, J. L.: O/C and OM/OC ratios of primary, secondary,  
947 and ambient organic aerosols with High-Resolution Time-of-Flight Aerosol Mass Spectrometry,  
948 *Environmental Science & Technology*, 42, 4478-4485, 10.1021/es703009q, 2008.
- 949 Almeida, S. M., Lage, J., Fernández, B., Garcia, S., Reis, M. A., and Chaves, P. C.: Chemical  
950 characterization of atmospheric particles and source apportionment in the vicinity of a steelmaking  
951 industry, *Science of The Total Environment*, 521-522, 411-420,  
952 <https://doi.org/10.1016/j.scitotenv.2015.03.112>, 2015.
- 953 Alzahrani, A. J., Alghamdi, A. G., and Ibrahim, H. M.: Assessment of soil loss due to wind erosion and  
954 dust deposition: Implications for sustainable management in arid regions, *Applied Sciences*, 14(23),  
955 10822, 10.3390/app142310822, 2024.
- 956 Amacher, G. S., Hyde, W. F., and Kanel, K. R.: Nepali fuelwood production and consumption: Regional  
957 and household distinctions, substitution and successful intervention, *The Journal of Development*  
958 *Studies*, 35, 138-163, 10.1080/00220389908422584, 1999.
- 959 Ambade, B., Sankar, T. K., Sahu, L. K., and Dumka, U. C.: Understanding sources and composition of  
960 black carbon and PM<sub>2.5</sub> in urban environments in East India, 10.3390/urbansci6030060, 2022.
- 961 Amato, F., Alastuey, A., de la Rosa, J., Gonzalez Castanedo, Y., Sánchez de la Campa, A. M., Pandolfi,  
962 M., Lozano, A., Contreras González, J., and Querol, X.: Trends of road dust emissions contributions

963 on ambient air particulate levels at rural, urban and industrial sites in southern Spain, *Atmospheric*  
964 *Chemistry and Physics*, 14, 3533-3544, 10.5194/acp-14-3533-2014, 2014.

965 Arimoto, R., Duce, R. A., Savoie, D. L., Prospero, J. M., Talbot, R., Cullen, J. D., Tomza, U., Lewis, N.  
966 F., and Ray, B. J.: Relationships among aerosol constituents from Asia and the North Pacific during  
967 PEM-West A, *Journal of Geophysical Research: Atmospheres*, 101, 2011-2023,  
968 <https://doi.org/10.1029/95JD01071>, 1996.

969 Arimoto, R., Duce, R. A., Savoie, D. L., Prospero, J. M., Talbot, R., Cullen, J. D., Tomza, U., Lewis, N.  
970 F., and Ray, B. J.: Relationships among aerosol constituents from Asia and the North Pacific during  
971 PEM-West A, *Journal of Geophysical Research: Atmospheres*, 101, 2011-2023,  
972 <https://doi.org/10.1029/95JD01071>, 1996.

973 Ashrafi, K., Fallah, R., Hadei, M., Yarahmadi, M., and Shahsavani, A.: Source apportionment of Total  
974 Suspended Particles (TSP) by Positive Matrix Factorization (PMF) and Chemical Mass Balance  
975 (CMB) modeling in Ahvaz, Iran, *Archives of Environmental Contamination and Toxicology*, 75,  
976 278-294, 10.1007/s00244-017-0500-z, 2018.

977 Bandowe, B. A. M., Nkansah, M. A., Leimer, S., Fischer, D., Lammel, G., and Han, Y.: Chemical (C, N,  
978 S, black carbon, soot and char) and stable carbon isotope composition of street dusts from a major  
979 West African metropolis: Implications for source apportionment and exposure, *Science of The Total*  
980 *Environment*, 655, 1468-1478, 10.1016/j.scitotenv.2018.11.089, 2019.

981 Barjoe, S. S., Abadi, S. Z. M., Elmi, M. R., Varaoon, V. T., and Nikbakht, M.: Evaluation of trace  
982 elements pollution in deposited dust on residential areas and agricultural lands around Pb/Zn  
983 mineral areas using modified pollution indices, *Journal of Environmental Health Science and*  
984 *Engineering*, 19, 753-769, 10.1007/s40201-021-00643-8, 2021.

985 Behera, B., Rahut, D. B., Jeetendra, A., and Ali, A.: Household collection and use of biomass energy  
986 sources in South Asia, *Energy*, 85, 468-480, 10.1016/j.energy.2015.03.059, 2015.

987 Belis, C. A., Pernigotti, D., Karagulian, F., Pirovano, G., Larsen, B. R., Gerboles, M., and Hopke, P. K.:  
988 A new methodology to assess the performance and uncertainty of source apportionment models in  
989 intercomparison exercises, *Atmospheric Environment*, 119, 35-44,  
990 <https://doi.org/10.1016/j.atmosenv.2015.08.002>, 2015.

991 Bond, T. C. and Bergstrom, R. W.: Light absorption by carbonaceous particles: An investigative review,  
992 *Aerosol Science and Technology*, 40, 27-67, 10.1080/02786820500421521, 2006.

993 Bond, T. C., Streets, D. G., Yarber, K. F., Nelson, S. M., Woo, J.-H., and Klimont, Z.: A technology-based  
994 global inventory of black and organic carbon emissions from combustion, *Journal of Geophysical*  
995 *Research: Atmospheres*, 109, <https://doi.org/10.1029/2003JD003697>, 2004.

996 Boreddy, S. K. R., Kawamura, K., Okuzawa, K., Kanaya, Y., and Wang, Z.: Temporal and diurnal  
997 variations of carbonaceous aerosols and major ions in biomass burning influenced aerosols over Mt.  
998 Tai in the North China Plain during MTX2006, *Atmospheric Environment*, 154, 106-117,  
999 <https://doi.org/10.1016/j.atmosenv.2017.01.042>, 2017.

1000 Bowen, H.-J.-M.: *Environmental chemistry of the elements*. Academic Press, 1979.

1001 Brooks, J., Liu, D., Allan, J. D., Williams, P. I., Haywood, J., Highwood, E. J., Kompalli, S. K., Babu, S.  
1002 S., Satheesh, S. K., Turner, A. G., and Coe, H.: Black carbon physical and optical properties across  
1003 northern India during pre-monsoon and monsoon seasons, *Atmospheric Chemistry and Physics*, 19,  
1004 13079-13096, [10.5194/acp-19-13079-2019](https://doi.org/10.5194/acp-19-13079-2019), 2019.

1005 Butler, K. M. and Mulholland, G. W.: Generation and transport of smoke components, *Fire Technology*,  
1006 40, 149-176, [10.1023/B:FIRE.0000016841.07530.64](https://doi.org/10.1023/B:FIRE.0000016841.07530.64), 2004.

1007 Cachier, H. and Ducret, J.: Influence of biomass burning on equatorial African rains, *Nature*, 352, 228-  
1008 230, [10.1038/352228a0](https://doi.org/10.1038/352228a0), 1991.

1009 Cao, J.-J., Wang, Q.-Y., Chow, J. C., Watson, J. G., Tie, X.-X., Shen, Z.-X., Wang, P., and An, Z.-S.:  
1010 Impacts of aerosol compositions on visibility impairment in Xi'an, China, *Atmospheric*  
1011 *Environment*, 59, 559-566, [10.1016/j.atmosenv.2012.05.036](https://doi.org/10.1016/j.atmosenv.2012.05.036), 2012a.

1012 Cao, J.: Characteristics of carbonaceous aerosol in Pearl River Delta Region, China during 2001 winter  
1013 period, *Atmospheric Environment*, 37, 1451-1460, [10.1016/s1352-2310\(02\)01002-6](https://doi.org/10.1016/s1352-2310(02)01002-6), 2003.

1014 Cao, J. J., Shen, Z. X., Chow, J. C., Watson, J. G., Lee, S. C., Tie, X. X., Ho, K. F., Wang, G. H., and  
1015 Han, Y. M.: Winter and summer PM<sub>2.5</sub> chemical compositions in fourteen Chinese cities, *Journal of*  
1016 *Air Waste Manage Association*, 62, 1214-1226, [10.1080/10962247.2012.701193](https://doi.org/10.1080/10962247.2012.701193), 2012b.

1017 Cao, J. J., Zhu, C. S., Tie, X. X., Geng, F. H., Xu, H. M., Ho, S. S. H., Wang, G. H., Han, Y. M., and Ho,  
1018 K. F.: Characteristics and sources of carbonaceous aerosols from Shanghai, China, *Atmospheric*  
1019 *Chemistry and Physics*, 13, 803-817, [10.5194/acp-13-803-2013](https://doi.org/10.5194/acp-13-803-2013), 2013.

1020 Casotti Rienda, I. and Alves, C. A.: Road dust resuspension: A review, *Atmospheric Research*, 261,  
1021 105740, <https://doi.org/10.1016/j.atmosres.2021.105740>, 2021.

1022 Cesari, D., Amato, F., Pandolfi, M., Alastuey, A., Querol, X., and Contini, D.: An inter-comparison of

1023 PM<sub>10</sub> source apportionment using PCA and PMF receptor models in three European sites,  
 1024 Environmental Science and Pollution Research, 23, 15133-15148, 10.1007/s11356-016-6599-z,  
 1025 2016.

1026 Chen, L., Zhang, X. Y., Tang, Q. L., Geng, Y., Wang, E. L., and Li, J. Y.: Heavy metal pollution and  
 1027 source analysis of surface soil in the Qaidam Basin (in Chinese), Environmental Science, 42, 4880–  
 1028 4888, <https://doi.org/10.13227/j.hjcx.202101052>, 2021.

1029 Chen, M., Li, M.-Y., Zhou, J.-Y., Fu, R.-B., Wang, X.-F., and Shen Z.: Characteristics and source analysis  
 1030 of heavy metal pollution in dust in a heavy industrial area of Northwest China (in Chinese),  
 1031 Environmental Science and Technology, 47(02), 155-164, 10.19672/j.cnki.1003-  
 1032 6504.1004.23.338, 2024.

1033 Chen, P., Kang, S., Bai, J., Sillanpää, M., and Li, C.: Yak dung combustion aerosols in the Tibetan Plateau:  
 1034 Chemical characteristics and influence on the local atmospheric environment, Atmospheric  
 1035 Research, 156, 58-66, 10.1016/j.atmosres.2015.01.001, 2015.

1036 Chen, W., Tong, D. Q., Dan, M., Zhang, S., Zhang, X., and Pan, Y.: Typical atmospheric haze during crop  
 1037 harvest season in northeastern China: A case in the Changchun region, Journal of Environmental  
 1038 Sciences, 54, 101-113, 10.1016/j.jes.2016.03.031, 2017.

1039 Cheng, X. and Lin, X.: Temporal and spatial distribution characteristics of dust in Shenyang and analysis  
 1040 of influencing factors (in Chinese). Environmental Protection Science 35(06), 1-3 + 58,  
 1041 10.16803/j.cnki.issn.1004-6216.2009.06.001, 2009.

1042 Chow, J. C.: Measurement methods to determine compliance with ambient air quality standards for  
 1043 suspended particles, Journal of the Air & Waste Management Association, 45, 320-382,  
 1044 10.1080/10473289.1995.10467369, 1995.

1045 Chow, J. C., Lowenthal, D. H., Chen, L. W. A., Wang, X., and Watson, J. G.: Mass reconstruction methods  
 1046 for PM<sub>2.5</sub>: A review, Air Quality, Atmosphere & Health, 8, 243-263, 10.1007/s11869-015-0338-3,  
 1047 2015.

1048 Chow, J. C., Watson, J. G., Kuhns, H., Etyemezian, V., Lowenthal, D. H., Crow, D., Kohl, S. D.,  
 1049 Engelbrecht, J. P., and Green, M. C.: Source profiles for industrial, mobile, and area sources in the  
 1050 Big Bend Regional Aerosol Visibility and Observational study, Chemosphere, 54, 185-208,  
 1051 10.1016/j.chemosphere.2003.07.004, 2004.

1052 Christie, J. A., Elliott, H. E., O’Connell-Lopez, S. M. O., Perry, K., Pratt, K. A., Hallar, A. G., Hrdina,

1053 A., Murphy, J. G., Riedel, T. P., Long, R. W., Mitroo, D., Haskins, J. D., and Gaston, C. J.: Halogen  
1054 production from playa dust emitted from the Great Salt Lake: Implications of the shrinking Great  
1055 Salt Lake on regional air quality, *ACS Earth and Space Chemistry*, 9, 480-493,  
1056 10.1021/acsearthspacechem.4c00258, 2025.

1057 Chuang, M.-T., Lee, C.-T., Chou, C. C. K., Lin, N.-H., Sheu, G.-R., Wang, J.-L., Chang, S.-C., Wang, S.-  
1058 H., Chi, K. H., Young, C.-Y., Huang, H., Chen, H.-W., Weng, G.-H., Lai, S.-Y., Hsu, S.-P., Chang,  
1059 Y.-J., Chang, J.-H., and Wu, X.-C.: Carbonaceous aerosols in the air masses transported from  
1060 Indochina to Taiwan: Long-term observation at Mt. Lulin, *Atmospheric Environment*, 89, 507-516,  
1061 10.1016/j.atmosenv.2013.11.066, 2014.

1062 Cichowicz, R. and Bochenek, A. D.: Assessing the effects of urban heat islands and air pollution on  
1063 human quality of life, *Anthropocene*, 46, 100433, <https://doi.org/10.1016/j.ancene.2024.100433>,  
1064 2024.

1065 Cong, Z., Kang, S., Luo, C., Li, Q., Huang, J., Gao, S., and Li, X.: Trace elements and lead isotopic  
1066 composition of PM<sub>10</sub> in Lhasa, Tibet, *Atmospheric Environment*, 45, 6210-6215,  
1067 <https://doi.org/10.1016/j.atmosenv.2011.07.060>, 2011.

1068 Dang, X., Chang, L., and Lu, N.: The impact of climatic warm-wet situation of the Tibetan Plateau on  
1069 the water resources and environment in Qaidam Basin, *Geology of China*, 46, 359-368, 2019.

1070 Demir, T., Karakaş, D., and Yenisoş-Karakaş, S.: Source identification of exhaust and non-exhaust traffic  
1071 emissions through the elemental carbon fractions and Positive Matrix Factorization method,  
1072 *Environmental Research*, 204, 112399, <https://doi.org/10.1016/j.envres.2021.112399>, 2022.

1073 Deng Z.-W., Fang, F. -M., Jiang, P.-L., Zhang J.-Q. and Lin Y.-S.: Distribution characteristics of black  
1074 carbon content in surface dust in Wuhu city (in Chinese), *Journal of Anqing Normal University*  
1075 (Natural Science Edition), 37(01), 58-62, 10.14182/j.cnki.1001-2443.2014.01.009, 2014.

1076 Dong, Z., Qin, D., Kang, S., Ren, J., Chen, J., Cui, X., Du, Z., and Qin, X.: Physicochemical  
1077 characteristics and sources of atmospheric dust deposition in snow packs on the glaciers of western  
1078 Qilian Mountains, China, *Tellus B: Chemical and Physical Meteorology*, 66, 20956,  
1079 10.3402/tellusb.v66.20956, 2014.

1080 Duan, J. and Tan, J.: Atmospheric heavy metals and Arsenic in China: Situation, sources and control  
1081 policies, *Atmospheric Environment*, 74, 93-101, 10.1016/j.atmosenv.2013.03.031, 2013.

1082 Eivazzadeh, M., Hassanvand, M. S., Faridi, S., and Gholampour, A.: Source apportionment and

1083 deposition of dustfall-bound trace elements around Tabriz, Iran, *Environmental Science and*  
1084 *Pollution Research International*, 28, 59403-59415, 10.1007/s11356-020-12173-1, 2021.

1085 Fan, Q., Cheng, Y., Chen, T., and Xu, N.: Influence of water replenishment of lakes in the Northern  
1086 Qaidam Basin on salt lake resources and ecological environment, *Journal of Salt Lake Research*, 30,  
1087 11-18, 2022.

1088 Fang, B., Zeng, H., Zhang, L., Wang, H., Liu, J., Hao, K., Zheng, G., Wang, M., Wang, Q., and Yang, W.:  
1089 Toxic metals in outdoor/indoor airborne PM<sub>2.5</sub> in port city of Northern, China: Characteristics,  
1090 sources, and personal exposure risk assessment, *Environmental Pollution*, 279, 116937,  
1091 <https://doi.org/10.1016/j.envpol.2021.116937>, 2021.

1092 Fang, H., Lowther, S. D., Zhu, M., Pei, C., Li, S., Fang, Z., Yu, X., Yu, Q., Wang, Y., Zhang, Y., Jones,  
1093 K. C., and Wang, X.: PM<sub>2.5</sub>-bound unresolved complex mixtures (UCM) in the Pearl River Delta  
1094 region: Abundance, atmospheric processes and sources, *Atmospheric Environment*, 226,  
1095 10.1016/j.atmosenv.2020.117407, 2020.

1096 Feng, W., Guo, Z., Xiao, X., Peng, C., Shi, L., Ran, H., and Xu, W.: Atmospheric deposition as a source  
1097 of cadmium and lead to soil-rice system and associated risk assessment, *Ecotoxicology and*  
1098 *Environmental Safety*, 180, 160-167, <https://doi.org/10.1016/j.ecoenv.2019.04.090>, 2019.

1099 Filonchyk, M., Yan, H., Yang, S., and Lu, X.: Detection of aerosol pollution sources during sandstorms  
1100 in Northwestern China using remote sensed and model simulated data, *Advances in Space Research*,  
1101 61, 1035-1046, <https://doi.org/10.1016/j.asr.2017.11.037>, 2018.

1102 Foyosal, M., Hossain, M., Rubaiyat, A., Sultana, S., Uddin, M. K., Sayem, M., and Akhter, J.: Household  
1103 energy consumption pattern in rural areas of Bangladesh, *Indian Journal of Energy*, 1, 72-85, 2012.

1104 Gao, G.-S., Song, L.-M., and Ma, Z.-T.: Temporal and spatial distribution of dust-fall in Qinghai Province  
1105 and analysis of its influencing factors (in Chinese), *Chinese Journal of Desert Research*, 33(04),  
1106 1124-1130, 2013.

1107 Gao, H. and Washington, R.: Arctic oscillation and the interannual variability of dust emissions from the  
1108 Tarim Basin: a TOMS AI based study, *Climate Dynamics*, 35, 511-522, 10.1007/s00382-009-0687-  
1109 4, 2010.

1110 Gao, Y., Wang, H., Yuan, L., Jing, S., Yuan, B., Shen, G., Zhu, L., Koss, A., Li, Y., Wang, Q., Huang, D.  
1111 D., Zhu, S., Tao, S., Lou, S., and Huang, C.: Measurement report: Underestimated reactive organic  
1112 gases from residential combustion – insights from a near-complete speciation, *Atmospheric*

1113 Chemistry and Physics, 23, 6633-6646, 10.5194/acp-23-6633-2023, 2023.

1114 Garaga, R., Gokhale, S., and Kota, S. H.: Source apportionment of size-segregated atmospheric particles  
1115 and the influence of particles deposition in the human respiratory tract in rural and urban locations  
1116 of north-east India, Chemosphere, 255, 10.1016/j.chemosphere.2020.126980, 2020.

1117 Gertler, A., Kuhns, H., Abu-Allaban, M., Damm, C., Gillies, J., Etyemezian, V., Clayton, R., and Proffitt,  
1118 D.: A case study of the impact of Winter road sand/salt and street sweeping on road dust re-  
1119 entrainment, Atmospheric Environment, 40, 5976-5985,  
1120 <https://doi.org/10.1016/j.atmosenv.2005.12.047>, 2006.

1121 Gholampour, A., Nabizadeh, R., Hassanvand, M. S., Taghipour, H., Nazmara, S., and Mahvi, A. H.:  
1122 Characterization of saline dust emission resulted from Urmia Lake drying, Journal of Environmental  
1123 Health Science & Engineering, 13, 82, 10.1186/s40201-015-0238-3, 2015.

1124 Gonçalves, C., Alves, C., Evtugina, M., Mirante, F., Pio, C., Caseiro, A., Schmidl, C., Bauer, H., and  
1125 Carvalho, F.: Characterisation of PM<sub>10</sub> emissions from woodstove combustion of common woods  
1126 grown in Portugal, Atmospheric Environment, 44, 4474-4480, <https://doi.org/10.1016/j.atmosenv.2010.08.047>,  
1127 2010.

1128 Gondwal, T. K. and Mandal, P.: Review on classification, sources and management of road dust and  
1129 determination of uncertainty associated with measurement of particle size of road dust, Mapan, 36,  
1130 909-924, 10.1007/s12647-021-00501-w, 2021.

1131 Gong, M., Yin, S., Gu, X., Xu, Y., Jiang, N., and Zhang, R.: Refined 2013-based vehicle emission  
1132 inventory and its spatial and temporal characteristics in Zhengzhou, China, Science of The Total  
1133 Environment, 599-600, 1149-1159, <https://doi.org/10.1016/j.scitotenv.2017.03.299>, 2017.

1134 Gray, H. A., Cass, G. R., Huntzicker, J. J., Heyerdahl, E. K., and Rau, J. A.: Characteristics of atmospheric  
1135 organic and elemental carbon particle concentrations in Los Angeles, Environmental Science &  
1136 Technology, 20, 580-589, 10.1021/es00148a006, 1986.

1137 Guo, J., Miao, Y., Zhang, Y., Liu, H., Li, Z., Zhang, W., He, J., Lou, M., Yan, Y., Bian, L., and Zhai, P.:  
1138 The climatology of planetary boundary layer height in China derived from radiosonde and  
1139 reanalysis data, Atmospheric Chemistry and Physics, 16, 13309-13319, 10.5194/acp-16-13309-2016,  
1140 2016.

1141 Guo, S., Wang, L., Zhou, P., Guo, S., Qin, W., An, S., Xiao, J.-Y., Liu, J., and Ji, Y.: Characteristics and  
1142 sources of organic carbon and elemental carbon in summer road dust in Shijiazhuang (in Chinese),

1143 Environmental Engineering, 36(04), 122-126, 10.13205/j.hjgc.201804025, 2018.

1144 Guo, W.-T., Zhao, F.-Q., and Chang, H.-L.: Analysis of the trend of environmental air quality changes in  
1145 the main urban area of Changzhi City (in Chinese), Proceedings of Shanghai, China 3, 2010.

1146 Gupta, A. and Dhir, A.: Assessment of air quality and chemical fingerprints for atmospheric fine aerosols  
1147 in an Indian smart city, Environmental Pollutants and Bioavailability, 34, 21-33,  
1148 10.1080/26395940.2021.2024091, 2022.

1149 Hahnenberger, M. and Nicoll, K.: Meteorological characteristics of dust storm events in the eastern Great  
1150 Basin of Utah, U.S.A, Atmospheric Environment, 60, 601-612, <https://doi.org/10.1016/j.atmosenv>,  
1151 2012.

1152 Hakanson, L.: An ecological risk index for aquatic pollution control. a sedimentological approach, Water  
1153 Research, 14, 975-1001, [https://doi.org/10.1016/0043-1354\(80\)90143-8](https://doi.org/10.1016/0043-1354(80)90143-8), 1980.

1154 Hama, S., Ouchen, I., Wyche, K. P., Cordell, R. L., and Monks, P. S.: Carbonaceous aerosols in five  
1155 European cities: Insights into primary emissions and secondary particle formation, Atmospheric  
1156 Research, 274, 10.1016/j.atmosres, 2022.

1157 Han, Y., Cao, J., An, Z., Chow, J. C., Watson, J. G., Jin, Z., Fung, K., and Liu, S.: Evaluation of the  
1158 thermal/optical reflectance method for quantification of elemental carbon in sediments,  
1159 Chemosphere, 69, 526-533, 10.1016/j.chemosphere, 2007a.

1160 Han, Y., Cao, J., Chow, J. C., Watson, J. G., An, Z., Jin, Z., Fung, K., and Liu, S.: Evaluation of the  
1161 thermal/optical reflectance method for discrimination between char- and soot-EC, Chemosphere,  
1162 69, 569-574, 10.1016/j.chemosphere, 2007b.

1163 Han, Y. M., Lee, S. C., Cao, J. J., Ho, K. F., and An, Z. S.: Spatial distribution and seasonal variation of  
1164 char-EC and soot-EC in the atmosphere over China, Atmospheric Environment, 43, 6066-6073,  
1165 10.1016/j.atmosenv, 2009a.

1166 Han, Y. M., Cao, J. J., Chow, J. C., Watson, J. G., An, Z. S., and Liu, S. X.: Elemental carbon in urban  
1167 soils and road dusts in Xi'an, China and its implication for air pollution, Atmospheric Environment,  
1168 43, 2464-2470, 10.1016/j.atmosenv, 2009b.

1169 Han, Y. M., Han, Z. W., Cao, J. J., Chow, J. C., Watson, J. G., An, Z. S., Liu, S. X., and Zhang, R. J.:  
1170 Distribution and origin of carbonaceous aerosol over a rural high-mountain lake area, Northern  
1171 China and its transport significance, Atmospheric Environment, 42, 2405-2414, 10.1016/j.atmosenv,  
1172 2008.

1173 Han, Y. M., Cao, J. J., Yan, B. Z., Kenna, T. C., Jin, Z. D., Cheng, Y., Chow, J. C., and An, Z. S.:  
1174 Comparison of elemental carbon in lake sediments measured by three different methods and 150-  
1175 year pollution history in Eastern China, *Environmental Science & Technology*, 45, 5287-5293,  
1176 10.1021/es103518c, 2011.

1177 Han, Y. M., Chen, L. W. A., Huang, R. J., Chow, J. C., Watson, J. G., Ni, H. Y., Liu, S. X., Fung, K. K.,  
1178 Shen, Z. X., Wei, C., Wang, Q. Y., Tian, J., Zhao, Z. Z., Prévôt, A. S. H., and Cao, J. J.: Carbonaceous  
1179 aerosols in megacity Xi'an, China: Implications of thermal/optical protocols comparison,  
1180 *Atmospheric Environment*, 132, 58-68, 10.1016/j.atmosenv, 2016.

1181 Hand, V. L., Capes, G., Vaughan, D. J., Formenti, P., Haywood, J. M., and Coe, H.: Evidence of internal  
1182 mixing of African dust and biomass burning particles by individual particle analysis using electron  
1183 beam techniques, *Journal of Geophysical Research: Atmospheres*, 115,  
1184 <https://doi.org/10.1029/2009JD012938>, 2010.

1185 He, B., Wang, J., Kong, F., Yu, D., Chen, L., Ling, Z., and Hu, J.: Analysis of environmental pollution  
1186 dissipation capacity of salt lake area in the Qaidam Basin, *Journal of Salt Lake Research*, 30, 52-60,  
1187 2022.

1188 He, L.-Y., Hu, M., Huang, X.-F., Yu, B.-D., Zhang, Y.-H., and Liu, D.-Q.: Measurement of emissions of  
1189 fine particulate organic matter from Chinese cooking, *Atmospheric Environment*, 38, 6557-6564,  
1190 10.1016/j.atmosenv, 2004.

1191 Heltberg, R., Arndt, T. C., and Sekhar, N. U.: Fuelwood consumption and forest degradation: A household  
1192 model for domestic energy substitution in rural India, *Land Economics*, 76, 213-232,  
1193 10.2307/3147225, 2000.

1194 Hilary, U., Efeoghene, E. A., Issac, A. O., Sami, R., Baakdah, F., and Pareek, S.: Exposure to airborne  
1195 pollutants in urban and rural areas: levels of metals and microorganisms in PM<sub>10</sub> and gaseous  
1196 pollutants in ambient air, *Air Quality, Atmosphere & Health*, 18, 317-332, 10.1007/s11869-024-  
1197 01644-w, 2025.

1198 Hoang, H. G., Chiang, C. F., Lin, C., Wu, C. Y., Lee, C. W., Cheruiyot, N. K., Tran, H. T., and Bui, X. T.:  
1199 Human health risk simulation and assessment of heavy metal contamination in a river affected by  
1200 industrial activities, *Environment Pollution*, 285, 117414, 10.1016/j.envpol.2021.117414, 2021.

1201 Hoeck, T., Droux, R., Breu, T., Hurni, H., and Maselli, D.: Rural energy consumption and land  
1202 degradation in a post-Soviet setting – an example from the west Pamir mountains in Tajikistan,

1203 Energy for Sustainable Development, 11, 48-57, [https://doi.org/10.1016/S0973-0826\(08\)60563-3](https://doi.org/10.1016/S0973-0826(08)60563-3),  
1204 2007.

1205 Hu, Y.-N. and Liu, Y.-L.: Characteristics and source analysis of heavy metal pollution in indoor dust in  
1206 Jinan (in Chinese). Environmental Science and Technology 45(06), 179-184, 10.19672/j.cnki.1003-  
1207 6504.0043.22.338, 2022.

1208 Hua, Y., Wang, S., Jiang, J., Zhou, W., Xu, Q., Li, X., Liu, B., Zhang, D., and Zheng, M.: Characteristics  
1209 and sources of aerosol pollution at a polluted rural site southwest in Beijing, China, Science of The  
1210 Total Environment, 626, 519-527, <https://doi.org/10.1016/j.scitotenv>, 2018.

1211 Huang, H., Xu, Z.-Q., Yan, J.-X., Zhao, X.-G., and Wang, D.-L.: Characteristics of heavy metal pollution  
1212 and ecological risk evaluation of indoor dust from urban and rural areas in Taiyuan City during the  
1213 heating season (in Chinese), Journal of Environmental Science, 42, 2143-2152,  
1214 10.13227/j.hjcx.202008045, 2021a.

1215 Huang, X., Tang, G., Zhang, J., Liu, B., Liu, C., Zhang, J., Cong, L., Cheng, M., Yan, G., Gao, W., Wang,  
1216 Y., and Wang, Y.: Characteristics of PM<sub>2.5</sub> pollution in Beijing after the improvement of air quality,  
1217 Journal of Environmental Sciences, 100, 1-10, <https://doi.org/10.1016/j.jes.2020.06.004>, 2021b.

1218 Huo, J., Ren, L., Pan, Y., Zhao, J., Xiang, X., Yu, C., Meng, D., Wang, Y., Lu, R., and Huang, Y.:  
1219 Functional traits of desert plants and their responses to environmental factors in Qaidam Basin,  
1220 China, Acta Ecologica Sinica, 42, 4494-4503, 2022.

1221 Ji, X., Xu, K., Liao, D., Chen, G., Liu, T., Hong, Y., Dong, S., Choi, S.-D., and Chen, J.: Spatial-temporal  
1222 characteristics and source apportionment of ambient VOCs in Southeast Mountain Area of China,  
1223 Aerosol And Air Quality Research, 22, 220016, 10.4209/aaqr. 220016, 2022.

1224 Jia, H., Yan, C., and Xing, X.: Evaluation of eco-environmental quality in Qaidam Basin based on the  
1225 Ecological Index (MRSEI) and GEE, Remote Sensing, 13, 10.3390/rs13224543, 2021.

1226 Jia, S.-M., Chen, M.-H., Yang, P.-F., Wang, L., Wang, G.-Y., Liu, L.-Y., and Ma, W.-L.: Seasonal  
1227 variations and sources of atmospheric EPFRs in a megacity in severe cold region: Implications for  
1228 the influence of strong coal and biomass combustion, Environmental Research, 252,  
1229 10.1016/j.envres.2024.119067, 2024.

1230 Jian, X., Guan, P., Fu, S.-T., Zhang, D.-W., Zhang, W., and Zhang, Y.-S.: Miocene sedimentary  
1231 environment and climate change in the northwestern Qaidam basin, northeastern Tibetan Plateau:  
1232 Facies, biomarker and stable isotopic evidences, Palaeogeography Palaeoclimatology

1233 Palaeoecology, 414, 320-331, 10.1016/j.palaeo.2014.09.011, 2014.

1234 Jiang, L., Xue, B., Xing, R., Chen, X., Song, L., Wang, Y., Coffman, D. M., and Mi, Z.: Rural household  
1235 energy consumption of farmers and herders in the Qinghai-Tibet Plateau, *Energy*, 192,  
1236 10.1016/j.energy.2019.116649, 2020.

1237 Jiang, Y., Shi, L., Guang, A. L., Mu, Z., Zhan, H., and Wu, Y.: Contamination levels and human health  
1238 risk assessment of toxic heavy metals in street dust in an industrial city in Northwest China,  
1239 *Environmental Geochemistry and Health*, 40, 2007-2020, 10.1007/s10653-017-0028-1, 2018.

1240 Joshi, U. M., Vijayaraghavan, K., and Balasubramanian, R.: Elemental composition of urban street dusts  
1241 and their dissolution characteristics in various aqueous media, *Chemosphere*, 77, 526-533,  
1242 10.1016/j.chemosphere, 2009.

1243 Kang, S., Zhang, Y., Qian, Y., and Wang, H.: A review of black carbon in snow and ice and its impact on  
1244 the cryosphere, *Earth-Science Reviews*, 210, 10.1016/j.earscirev.2020.103346, 2020.

1245 Karimian Torghabeh, A., Jahandari, A., and Jamasb, R.: Concentration, contamination level, source  
1246 identification of selective trace elements in Shiraz atmospheric dust sediments (Fars Province, SW  
1247 Iran), *Environmental Science and Pollution Research (International)*, 26, 6424-6435,  
1248 10.1007/s11356-018-04100-2, 2019.

1249 Katakai, R., Goswami, K., Bordoloi, N. J., Narzari, R., Saikia, R., Sut, D., and Gogoi, L.: Biomass  
1250 resources for biofuel production in Northeast India, in: *Bioprospecting of indigenous bioresources  
1251 of North-East India*, edited by: Purkayastha, J., Springer Singapore, Singapore, 127-151,  
1252 10.1007/978-981-10-0620-3\_8, 2016.

1253 Kerimray, A., Suleimenov, B., De Miglio, R., Rojas-Solórzano, L., Amouei Torkmahalleh, M., and Ó  
1254 Gallachóir, B. P.: Investigating the energy transition to a coal free residential sector in Kazakhstan  
1255 using a regionally disaggregated energy systems model, *Journal of Cleaner Production*, 196, 1532-  
1256 1548, <https://doi.org/10.1016/j.jclepro>, 2018.

1257 Khan, A. J., Swami, K., Ahmed, T., Bari, A., Shareef, A., and Husain, L.: Determination of elemental  
1258 carbon in lake sediments using a thermal-optical transmittance (TOT) method, *Atmospheric  
1259 Environment*, 43, 5989-5995, <https://doi.org/10.1016/j.atmosenv.2009.08.030>, 2009.

1260 Kim, K. H., Sekiguchi, K., Kudo, S., and Sakamoto, K.: Characteristics of atmospheric elemental carbon  
1261 (Char and Soot) in ultrafine and fine particles in a roadside environment, Japan, *Aerosol and Air  
1262 Quality Research*, 11, 1-12, 10.4209/aaqr.2010.07.0061, 2011.

1263 Kulmala, M., Vehkamäki, H., Petäjä, T., Dal Maso, M., Lauri, A., Kerminen, V. M., Birmili, W., and  
1264 McMurry, P. H.: Formation and growth rates of ultrafine atmospheric particles: a review of  
1265 observations, *Journal of Aerosol Science*, 35, 143-176,  
1266 <https://doi.org/10.1016/j.jaerosci.2003.10.003>, 2004.

1267 Kumar, A.: Chemical characterization of mineral aerosols: Sources, transport and atmospheric  
1268 transformations, Mohanlal Sukhadia University Udaipur, 2010.

1269 Kumar, N., Johnson, J., Yarwood, G., Woo, J.-H., Kim, Y., Park, R. J., Jeong, J. I., Kang, S., Chun, S.,  
1270 and Knipping, E.: Contributions of domestic sources to PM<sub>2.5</sub> in South Korea, *Atmospheric*  
1271 *Environment*, 287, 119273, <https://doi.org/10.1016/j.atmosenv.2022.119273>, 2022.

1272 Lai, S., Zhao, Y., Ding, A., Zhang, Y., Song, T., Zheng, J., Ho, K. F., Lee, S.-c., and Zhong, L.:  
1273 Characterization of PM<sub>2.5</sub> and the major chemical components during a 1-year campaign in rural  
1274 Guangzhou, Southern China, *Atmospheric Research*, 167, 208-215, [10.1016/j.atmosres](https://doi.org/10.1016/j.atmosres.2016.07.011), 2016.

1275 Leavey, A., Patel, S., Martinez, R., Mitroo, D., Fortenberry, C., Walker, M., Williams, B., and Biswas, P.:  
1276 Organic and inorganic speciation of particulate matter formed during different combustion phases  
1277 in an improved cookstove, *Environmental Research*, 158, 33-42, [10.1016/j.envres](https://doi.org/10.1016/j.envres.2017.07.011), 2017.

1278 Lee, K. Y., Batmunkh, T., Joo, H. S., and Park, K.: Comparison of the physical and chemical  
1279 characteristics of fine road dust at different urban sites, *Journal of the Air & Waste Management*  
1280 *Association*, 68, 812-823, [10.1080/10962247.2018.1443855](https://doi.org/10.1080/10962247.2018.1443855), 2018.

1281 Li, J.-K., Liu, X.-F. and Wang, D.-H.: Overview of mineralization laws of lithium deposits in China (in  
1282 Chinese). *Acta Geologica Sinica*, 88: 2269-2283. DOI: [10.19762/j.cnki.dizhixuebao](https://doi.org/10.19762/j.cnki.dizhixuebao.2014.04.001), 2014.

1283 Li, L., Ni, W., Cheng, Y., Wang, H., Yuan, K., and Zhou, B.: Evaluation of the eco-geo-environment in  
1284 the Qaidam Basin, China, *Environmental Earth Sciences*, 80, [10.1007/s12665-020-09312-9](https://doi.org/10.1007/s12665-020-09312-9), 2021a.

1285 Li, M., Liu, Z., Chen, J., Huang, X., Liu, J., Xie, Y., Hu, B., Xu, Z., Zhang, Y., and Wang, Y.:  
1286 Characteristics and source apportionment of metallic elements in PM<sub>2.5</sub> at urban and suburban sites  
1287 in Beijing: Implication of emission reduction, *Atmosphere*, 10, [10.3390/atmos10030105](https://doi.org/10.3390/atmos10030105), 2019.

1288 Li, P.-h., Wang, Y., Li, T., Sun, L., Yi, X., Guo, L.-q., and Su, R.-h.: Characterization of carbonaceous  
1289 aerosols at Mount Lu in South China: implication for secondary organic carbon formation and long-  
1290 range transport, *Environmental Science and Pollution Research*, 22, 14189-14199, [10.1007/s11356-](https://doi.org/10.1007/s11356-015-4654-9)  
1291 [015-4654-9](https://doi.org/10.1007/s11356-015-4654-9), 2015b.

1292 Li, Q.-L and Sha, Z.-J.: Remote sensing monitoring of ecological environment quality in the Qaidam

1293 Basin under climate warming (in Chinese), *Ecological Science*, 41(06), 92-99,  
1294 10.14108/j.cnki.1008-8873, 2022.

1295 Li, R., Li, C., Zhuang, J., Zhu, H., Fang, L., and Sun, D.: Mechanistic influence of chemical  
1296 agglomeration agents on removal of inhalable particles from coal combustion, *ACS Omega*, 5,  
1297 25906-25912, 10.1021/acsomega.0c03263, 2020.

1298 Li, Y., Ma, L., Ge, Y., and Abuduwaili, J.: Health risk of heavy metal exposure from dustfall and source  
1299 apportionment with the PCA-MLR model: A case study in the Ebinur Lake Basin, China,  
1300 *Atmospheric Environment*, 272, 118950, <https://doi.org/10.1016/j.atmosenv>, 2022.

1301 Li, Z., Liu, J., Zhai, Z., Liu, C., Ren, Z., Yue, Z., Yang, D., Hu, Y., Zheng, H., and Kong, S.:  
1302 Heterogeneous changes of chemical compositions, sources and health risks of PM<sub>2.5</sub> with the "Clean  
1303 Heating" policy at urban/suburban/industrial sites, *Science of The Total Environment*, 854, 158871,  
1304 10.1016/j.scitotenv.2022.158871, 2023.

1305 Li, Z., Yue, Z., Yang, D., Wang, L., Wang, X., Li, Z., Wang, Y., Chen, L., Guo, S., Yao, J., Lou, X., Xu,  
1306 X., and Wei, J.: Levels, chemical compositions, and sources of PM<sub>2.5</sub> of rural and urban area under  
1307 the impact of wheat harvest, *Aerosol and Air Quality Research*, 21, 10.4209/aaqr.210026, 2021.

1308 Lin, Y. C., Tsai, C. J., Wu, Y. C., Zhang, R., Chi, K. H., Huang, Y. T., Lin, S. H., and Hsu, S. C.:  
1309 Characteristics of trace metals in traffic-derived particles in Hsuehshan Tunnel, Taiwan: size  
1310 distribution, potential source, and fingerprinting metal ratio, *Atmospheric Chemistry and Physics*,  
1311 15, 4117-4130, 10.5194/acp-15-4117-2015, 2015.

1312 Liu, B., Song, N., Dai, Q., Mei, R., Sui, B., Bi, X., and Feng, Y.: Chemical composition and source  
1313 apportionment of ambient PM<sub>2.5</sub> during the non-heating period in Taian, China, *Atmospheric  
1314 Research*, 170, 23-33, 10.1016/j.atmosres, 2016a.

1315 Liu, G., Lucas, M., and Shen, L.: Rural household energy consumption and its impacts on eco-  
1316 environment in Tibet: Taking Taktse county as an example, *Renewable and Sustainable Energy  
1317 Reviews*, 12, 1890-1908, <https://doi.org/10.1016/j.rser>, 2008.

1318 Liu, G., Li, J., Wu, D., and Xu, H.: Chemical composition and source apportionment of the ambient PM<sub>2.5</sub>  
1319 in Hangzhou, China, *Particuology*, 18, 135-143, <https://doi.org/10.1016/j.partic>, 2015.

1320 Liu, G., Yin, G., Kurban, A., Aishan, T., and You, H.: Spatiotemporal dynamics of land cover and their  
1321 impacts on potential dust source regions in the Tarim Basin, NW China, *Environmental Earth  
1322 Sciences*, 75, 1477, 10.1007/s12665-016-6269-y, 2016b.

1323 Liu, H., Hu, B., Zhang, L., Zhao, X. J., Shang, K. Z., Wang, Y. S., and Wang, J.: Ultraviolet radiation  
1324 over China: Spatial distribution and trends, *Renewable and Sustainable Energy Reviews*, 76, 1371-  
1325 1383, [https://doi.org/10.1016/j.rser](https://doi.org/10.1016/j.rser.2017), 2017.

1326 Liu, P., Zhou, H., Chun, X., Wan, Z., Liu, T., Sun, B., Wang, J., and Zhang, W.: Characteristics of fine  
1327 carbonaceous aerosols in Wuhai, a resource-based city in Northern China: Insights from energy  
1328 efficiency and population density, *Environmental Pollution*, 292, 118368,  
1329 [https://doi.org/10.1016/j.envpol](https://doi.org/10.1016/j.envpol.2022), 2022.

1330 Liu, T., Zhao, C., Chen, Q., Li, L., Si, G., Li, L., and Guo, B.: Characteristics and health risk assessment  
1331 of heavy metal pollution in atmospheric particulate matter in different regions of the Yellow River  
1332 Delta in China, *Environmental Geochemistry and Health*, 45, 2013-2030, 10.1007/s10653-022-  
1333 01318-5, 2023b.

1334 Liu, W., Hopke, P. K., Han, Y.-j., Yi, S.-M., Holsen, T. M., Cybart, S., Kozlowski, K., and Milligan, M.:  
1335 Application of receptor modeling to atmospheric constituents at Potsdam and Stockton, NY,  
1336 *Atmospheric Environment*, 37, 4997-5007, <https://doi.org/10.1016/j.atmosenv.2003.08.036>, 2003.

1337 Liu, X., Wang, Y., Liu, R., Zhang, Y., Shao, L., Han, K., and Zhang, Y.: Pollution characteristics, source  
1338 identification and potential ecological risk of 50 elements in atmospheric particulate matter during  
1339 winter in Qingdao, *Arabian Journal of Geosciences*, 15, 10.1007/s12517-022-09521-5, 2022b.

1340 Liu, Y., Liu, G., Yousaf, B., Zhang, J., and Zhou, L.: Carbon fractionation and stable carbon isotopic  
1341 fingerprint of road dusts near coal power plant with emphases on coal-related source apportionment,  
1342 *Ecotoxicology and Environmental Safety*, 202, 110888, [https://doi.org/10.1016/j.ecoenv](https://doi.org/10.1016/j.ecoenv.2020a), 2020a.

1343 Liu, Y., Wu, G., Duan, A. and Zhang, Q.: New evidence that climate warming in the Tibetan Plateau is a  
1344 result of intensified greenhouse gas emissions (in Chinese), *Chinese Science Bulletin*, 51(8), 989-  
1345 992, 10.1360/csb2006-51-8-989, 2006.

1346 Liu, Y., Zhu, Q., Huang, J., Hua, S., and Jia, R.: Impact of dust-polluted convective clouds over the  
1347 Tibetan Plateau on downstream precipitation, *Atmospheric Environment*, 209, 67-77,  
1348 [https://doi.org/10.1016/j.atmosenv](https://doi.org/10.1016/j.atmosenv.2019), 2019.

1349 Liu, Y., Zhu, Q., Hua, S., Alam, K., Dai, T., and Cheng, Y.: Tibetan Plateau driven impact of Taklimakan  
1350 dust on northern rainfall, *Atmospheric Environment*, 234, 117583,  
1351 [https://doi.org/10.1016/j.atmosenv](https://doi.org/10.1016/j.atmosenv.2020b), 2020b.

1352 Liu, Z. Y., Cheng, J. L., Li, C. Y., Gao, Y., Zhan, C. L., Liu, S., Zhang, J. Q., and Liu, H. X.: Pollution

1353 characteristics and source analysis of carbon components in road dust from Qingshan District,  
1354 Wuhan (in Chinese), *Environmental Chemistry*, 40, 772–778, 2021.

1355 Lonati, G., Ozgen, S., and Giugliano, M.: Primary and secondary carbonaceous species in PM<sub>2.5</sub> samples  
1356 in Milan (Italy), *Atmospheric Environment*, 41, 4599-4610, <https://doi.org/10.1016/j.atmosenv>,  
1357 2007.

1358 Löw, F., Navratil, P., Kotte, K., Schöler, H. F., and Bubenzer, O.: Remote-sensing-based analysis of  
1359 landscape change in the desiccated seabed of the Aral Sea—a potential tool for assessing the hazard  
1360 degree of dust and salt storms, *Environmental Monitoring and Assessment*, 185, 8303-8319,  
1361 10.1007/s10661-013-3174-7, 2013.

1362 Luo, M., Liu, Y., Zhu, Q., Tang, Y., and Alam, K.: Role and mechanisms of black carbon affecting water  
1363 vapor transport to Tibet, *Remote Sensing*, 12(2), 0231, 10.3390/rs12020231, 2020.

1364 Ma, Q., Wu, Y., Tao, J., Xia, Y., Liu, X., Zhang, D., Han, Z., Zhang, X., and Zhang, R.: Variations of  
1365 chemical composition and source apportionment of PM<sub>2.5</sub> during winter haze episodes in Beijing,  
1366 *Aerosol and Air Quality Research*, 17, 2791-2803, 10.4209/aaqr.2017.10.0366, 2017.

1367 Ma, Y., Ji, Y.-Q., Guo, J.-J., Zhao, J.-Q., Li, Y.-Y., Wang, S.-B. and Zhang, L.: Characteristics of carbon  
1368 components and source analysis of road dust during spring in Tianjin (in Chinese), *Acta Scientiae*  
1369 *Circumstantiae* 40(06), 2540-2545, 10.13227/j.hjkx, 2019.

1370 Manousakas, M., Papaefthymiou, H., Diapouli, E., Migliori, A., Karydas, A. G., Bogdanovic-Radovic,  
1371 I., and Eleftheriadis, K.: Assessment of PM<sub>2.5</sub> sources and their corresponding level of uncertainty  
1372 in a coastal urban area using EPA PMF 5.0 enhanced diagnostics, *Science of The Total Environment*,  
1373 574, 155-164, 10.1016/j.scitotenv.2016.09.047, 2017.

1374 Mbengue, S., Fusek, M., Schwarz, J., Vodička, P., Šmejkalová, A. H., and Holoubek, I.: Four years of  
1375 highly time resolved measurements of elemental and organic carbon at a rural background site in  
1376 Central Europe, *Atmospheric Environment*, 182, 335-346, 10.1016/j.atmosenv, 2018.

1377 Meng, J.-H., Shi, X.-F., Xiang, Y. and Ren, Y.-F.: Current status and sources of heavy metal pollution in  
1378 the atmosphere (in Chinese). *Environmental Science and Management* 42(08), 51-53, 2017.

1379 Meng, W., Zhong, Q., Chen, Y., Shen, H., Yun, X., Smith, K. R., Li, B., Liu, J., Wang, X., Ma, J., Cheng,  
1380 H., Zeng, E. Y., Guan, D., Russell, A. G., and Tao, S.: Energy and air pollution benefits of household  
1381 fuel policies in northern China, *Proceedings of the National Academy of Sciences*, 116, 16773-  
1382 16780, 10.1073/pnas.1904182116, 2019.

1383 Meng, W., Shen, H., Yun, X., Chen, Y., Zhong, Q., Zhang, W., Yu, X., Xu, H., Ren, Y. a., Shen, G., Ma,  
1384 J., Liu, J., Cheng, H., Wang, X., Zhu, D., and Tao, S.: Differentiated-rate clean heating strategy with  
1385 superior environmental and health benefits in Northern China, *Environmental Science &*  
1386 *Technology*, 54, 13458-13466, 10.1021/acs.est.0c04019, 2020.

1387 Miller, M. B., Fine, R., Pierce, A. M., and Gustin, M. S.: Identifying sources of ozone to three rural  
1388 locations in Nevada, USA, using ancillary gas pollutants, aerosol chemistry, and mercury, *Science*  
1389 *of The Total Environment*, 530-531, 483-492, <https://doi.org/10.1016/j.scitotenv>, 2015.

1390 Millet, D. B., Donahue, N. M., Pandis, S. N., Polidori, A., Stanier, C. O., Turpin, B. J., and Goldstein, A.  
1391 H.: Atmospheric volatile organic compound measurements during the Pittsburgh Air Quality Study:  
1392 Results, interpretation, and quantification of primary and secondary contributions, *Journal of*  
1393 *Geophysical Research: Atmospheres*, 110, <https://doi.org/10.1029/2004JD004601>, 2005.

1394 Ming, J., Xiao, C., Sun, J., Kang, S., and Bonasoni, P.: Carbonaceous particles in the atmosphere and  
1395 precipitation of the Nam Co region, central Tibet, *Journal of Environmental Sciences*, 22, 1748-  
1396 1756, [https://doi.org/10.1016/S1001-0742\(09\)60315-6](https://doi.org/10.1016/S1001-0742(09)60315-6), 2010.

1397 Mishra, M. and Kulshrestha, U.: Chemical characteristics and deposition fluxes of dust-carbon mixed  
1398 coarse aerosols at three sites of Delhi, NCR, *Journal of Atmospheric Chemistry*, 74, 399-421,  
1399 10.1007/s10874-016-9349-1, 2017.

1400 Moravek, A., Murphy, J. G., Hrdina, A., Lin, J. C., Pennell, C., Franchin, A., Middlebrook, A. M., Fibiger,  
1401 D. L., Womack, C. C., McDuffie, E. E., Martin, R., Moore, K., Baasandorj, M., and Brown, S. S.:  
1402 Wintertime spatial distribution of ammonia and its emission sources in the Great Salt Lake region,  
1403 *Atmospheric Chemistry and Physics*, 19, 15691-15709, 10.5194/acp-19-15691-2019, 2019.

1404 Muller, G.: Index of geoaccumulation in sediments of the rhine river, *GeoJournal*, 2, 108-118, 1969.

1405 Munawer, M. E.: Human health and environmental impacts of coal combustion and post-combustion  
1406 wastes, *Journal of Sustainable Mining*, 17, 87-96, <https://doi.org/10.1016/j.jsm>, 2018.

1407 Na, K., Sawant, A. A., Song, C., and Cocker, D. R.: Primary and secondary carbonaceous species in the  
1408 atmosphere of Western Riverside County, California, *Atmospheric Environment*, 38, 1345-1355,  
1409 10.1016/j.atmosenv, 2004.

1410 Nuralkyzy, B., Wang, P., Deng, X., An, S., and Huang, Y.: Heavy metal contents and assessment of soil  
1411 contamination in different land-use types in the Qaidam Basin, *Sustainability*, 13(21), 12020,  
1412 10.3390/su132112020, 2021.

1413 Qi, D.-L., Zhao, Q.-N., Zhao, H.-F., Han, T.-F. and Su, W.-J.: Temporal and spatial characteristics and  
1414 regional differences of dust-fall in Qinghai Province from 2004 to 2017 (in Chinese), *Arid*  
1415 *Meteorology*, 36(06), 927-935, 2018.

1416 Qian, G.-Q. and Dong, Z.-B.: Research on methods and related issues of atmospheric dust collection (in  
1417 Chinese), *Chinese Journal of Desert Research*, (06), 119-122, 2014.

1418 Oliveira, T., Pio, C., Alves, C., Silvestre, A., Evtyugina, M., Afonso, J., Caseiro, A., and Legrand, M.:  
1419 Air quality and organic compounds in aerosols from a coastal rural area in the Western Iberian  
1420 Peninsula over a year long period: Characterisation, loads and seasonal trends, *Atmospheric*  
1421 *Environment*, 41, 3631-3643, 10.1016/j.atmosenv, 2007.

1422 Pacyna, J. M. and Pacyna, E. G.: An assessment of global and regional emissions of trace metals to the  
1423 atmosphere from anthropogenic sources worldwide, *Environmental Reviews*, 9, 269-298,  
1424 10.1139/a01-012, 2001.

1425 Pandolfi, M., Gonzalez-Castanedo, Y., Alastuey, A., de la Rosa, J. D., Mantilla, E., de la Campa, A. S.,  
1426 Querol, X., Pey, J., Amato, F., and Moreno, T.: Source apportionment of PM<sub>10</sub> and PM<sub>2.5</sub> at multiple  
1427 sites in the strait of Gibraltar by PMF: impact of shipping emissions, *Environmental Science and*  
1428 *Pollution Research*, 18, 260-269, 10.1007/s11356-010-0373-4, 2010.

1429 Pervez, S., Bano, S., Watson, J. G., Chow, J. C., Matawle, J. L., Shrivastava, A., Tiwari, S., and Pervez,  
1430 Y. F.: Source profiles for PM<sub>10-2.5</sub> resuspended dust and vehicle exhaust emissions in Central India,  
1431 *Aerosol and Air Quality Research*, 18, 1660-1672, 10.4209/aaqr, 2018.

1432 Phairuang, W., Hongtieab, S., Suwattiga, P., Furuuchi, M., and Hata, M.: Atmospheric Ultrafine  
1433 Particulate Matter (PM<sub>0.1</sub>)-bound carbon composition in Bangkok, Thailand, *Atmosphere*, 13,  
1434 10.3390/atmos13101676, 2022.

1435 Pio, C., Cerqueira, M., Harrison, R. M., Nunes, T., Mirante, F., Alves, C., Oliveira, C., Sanchez de la  
1436 Campa, A., Artíñano, B., and Matos, M.: OC/EC ratio observations in Europe: Re-thinking the  
1437 approach for apportionment between primary and secondary organic carbon, *Atmospheric*  
1438 *Environment*, 45, 6121-6132, 10.1016/j.atmosenv, 2011.

1439 Pipal, A. S., Singh, S., and Satsangi, G. P.: Study on bulk to single particle analysis of atmospheric  
1440 aerosols at urban region, *Urban Climate*, 27, 243-258, <https://doi.org/10.1016/j.uclim.2018.12.008>,  
1441 2019.

1442 Popovicheva, O. B., Engling, G., Diapouli, E., Saraga, D., Persiantseva, N. M., Timofeev, M. A., Kireeva,

1443 E. D., Shonija, N. K., Chen, S.-H., Nguyen, D. L., Eleftheriadis, K., and Lee, C.-T.: Impact of smoke  
1444 intensity on size-resolved aerosol composition and microstructure during the biomass burning  
1445 season in Northwest Vietnam, *Aerosol and Air Quality Research*, 16, 2635-2654, 10.4209/aaqr,  
1446 2016.

1447 Qiao, Q., Huang, B., Zhang, C., Piper, J. D. A., Pan, Y., and Sun, Y.: Assessment of heavy metal  
1448 contamination of dustfall in northern China from integrated chemical and magnetic investigation,  
1449 *Atmospheric Environment*, 74, 182-193, 10.1016/j.atmosenv, 2013.

1450 Rogge, W. F., Hildemann, L. M., Mazurek, M. A., Cass, G. R., and Simoneit, B. R. T.: Sources of fine  
1451 organic aerosol. 3. Road dust, tire debris, and organometallic brake lining dust: roads as sources and  
1452 sinks, *Environmental Science & Technology*, 27, 1892-1904, 10.1021/es00046a019, 1993.Safai, P.  
1453 D., Raju, M. P., Rao, P. S. P., and Pandithurai, G.: Characterization of carbonaceous aerosols over  
1454 the urban tropical location and a new approach to evaluate their climatic importance, *Atmospheric  
1455 Environment*, 92, 493-500, 10.1016/j.atmosenv.2014.04.055, 2014.

1456 Schmidl, C., Marr, I. L., Caseiro, A., Kotianová, P., Berner, A., Bauer, H., Kasper-Giebl, A., and Puxbaum,  
1457 H.: Chemical characterisation of fine particle emissions from wood stove combustion of common  
1458 woods growing in mid-European Alpine regions, *Atmospheric Environment*, 42, 126-141,  
1459 <https://doi.org/10.1016/j.atmosenv>, 2008.

1460 Secrest, M. H., Schauer, J. J., Carter, E. M., and Baumgartner, J.: Particulate matter chemical component  
1461 concentrations and sources in settings of household solid fuel use, *Indoor Air*, 27, 1052-1066,  
1462 10.1111/ina.12389, 2017.

1463 Seinfeld, J. H., Pandis, S. N., and Noone, K. J. J. P. T.: Atmospheric chemistry and physics: From air  
1464 pollution to climate change, 51, 88-90, 1998.

1465 Sheehan, P. E. and Bowman, F. M.: Estimated effects of temperature on secondary organic aerosol  
1466 concentrations, *Environmental Science & Technology*, 35, 2129-2135, 10.1021/es001547g, 2001.

1467 Shen, J. and Dai, B. L.: Development and utilization of salt lake brine lithium resources and its prospects  
1468 (in Chinese), *Industrial Minerals & Processing*, 38, 1-4+7,  
1469 <https://doi.org/10.16283/j.cnki.hgkwyjg.2009.04.004>, 2009.

1470 Shen, G.-F., Xiong, R., Cheng, H.-F. and Tao, S.: Estimation of residential energy structure and primary  
1471 PM<sub>2.5</sub> emissions in rural Tibet (in Chinese), *Science Bulletin*, 66(15), 1900-1911, 2021.

1472 Shen, Z., Arimoto, R., Cao, J., Zhang, R., Li, X., Du, N., Okuda, T., Nakao, S., and Tanaka, S.: Seasonal

1473 variations and evidence for the effectiveness of pollution controls on water-soluble inorganic species  
1474 in total suspended particulates and fine particulate matter from Xi'an, China, *Journal of the Air &*  
1475 *Waste Management Association*, 58, 1560-1570, 10.3155/1047-3289.58.12.1560, 2008.

1476 Shi, G., Chen, Z., Teng, J., Bi, C., Zhou, D., Sun, C., Li, Y., and Xu, S.: Fluxes, variability and sources  
1477 of cadmium, lead, arsenic and mercury in dry atmospheric depositions in urban, suburban and rural  
1478 areas, *Environmental Research*, 113, 28-32, <https://doi.org/10.1016/j.envres.2012.01.001>, 2012.

1479 Shi, X., Zhao, Y., Dai, S., Xu, L., Li, Y., Jia, H., and Zhang, Q.: Research on climatic change of Qaidam  
1480 Basin since 1961, *Journal of Desert Research*, 25, 123-128, 2005.

1481 Shi, Z., Vu, T., Kotthaus, S., Harrison, R. M., Grimmond, S., Yue, S., Zhu, T., Lee, J., Han, Y., Demuzere,  
1482 M., Dunmore, R. E., Ren, L., Liu, D., Wang, Y., Wild, O., Allan, J., Acton, W. J., Barlow, J., Barratt,  
1483 B., Beddows, D., Bloss, W. J., Calzolari, G., Carruthers, D., Carslaw, D. C., Chan, Q., Chatzidiakou,  
1484 L., Chen, Y., Crilley, L., Coe, H., Dai, T., Doherty, R., Duan, F., Fu, P., Ge, B., Ge, M., Guan, D.,  
1485 Hamilton, J. F., He, K., Heal, M., Heard, D., Hewitt, C. N., Hollaway, M., Hu, M., Ji, D., Jiang, X.,  
1486 Jones, R., Kalberer, M., Kelly, F. J., Kramer, L., Langford, B., Lin, C., Lewis, A. C., Li, J., Li, W.,  
1487 Liu, H., Liu, J., Loh, M., Lu, K., Lucarelli, F., Mann, G., McFiggans, G., Miller, M. R., Mills, G.,  
1488 Monk, P., Nemitz, E., O'Connor, F., Ouyang, B., Palmer, P. I., Percival, C., Popoola, O., Reeves, C.,  
1489 Rickard, A. R., Shao, L., Shi, G., Spracklen, D., Stevenson, D., Sun, Y., Sun, Z., Tao, S., Tong, S.,  
1490 Wang, Q., Wang, W., Wang, X., Wang, X., Wang, Z., Wei, L., Whalley, L., Wu, X., Wu, Z., Xie, P.,  
1491 Yang, F., Zhang, Q., Zhang, Y., Zhang, Y., and Zheng, M.: Introduction to the special issue "In-depth  
1492 study of air pollution sources and processes within Beijing and its surrounding region (APHH-  
1493 Beijing)", *Atmospheric Chemistry and Physics*, 19, 7519-7546, 10.5194/acp-19-7519-2019, 2019.

1494 Simoneit, B. R. T.: Biomass burning — a review of organic tracers for smoke from incomplete  
1495 combustion, *Applied Geochemistry*, 17, 129-162, [https://doi.org/10.1016/S0883-2927\(01\)00061-0](https://doi.org/10.1016/S0883-2927(01)00061-0),  
1496 2002.

1497 Smichowski, P., Gómez, D., Frazzoli, C., and Caroli, S.: Traffic-related elements in airborne particulate  
1498 matter, *Applied Spectroscopy Reviews*, 43, 23-49, 10.1080/05704920701645886, 2007.

1499 Song, P. S., Li, W., Sun, B., Nie, Z., Bu, L. Z., and Wang, Y. S.: Progress in the development and  
1500 utilization of salt lake resources (in Chinese), *Journal of Inorganic Chemistry*, 27, 801-815,  
1501 2011.

1502 Sow, M., Goossens, D., and Rajot, J. L.: Calibration of the MDCO dust collector and of four versions of

1503 the inverted frisbee dust deposition sampler, *Geomorphology*, 82, 360-375,  
 1504 10.1016/j.geomorph.2006.05.013, 2006.

1505 Strader, R., Lurmann, F., and Pandis, S. N.: Evaluation of secondary organic aerosol formation in winter,  
 1506 *Atmospheric Environment*, 33, 4849-4863, [https://doi.org/10.1016/S1352-2310\(99\)00310-6](https://doi.org/10.1016/S1352-2310(99)00310-6), 1999.

1507 Sulong, N. A., Latif, M. T., Sahani, M., Khan, M. F., Fadzil, M. F., Tahir, N. M., Mohamad, N., Sakai,  
 1508 N., Fujii, Y., Othman, M., and Tohno, S.: Distribution, sources and potential health risks of  
 1509 polycyclic aromatic hydrocarbons (PAHs) in PM<sub>2.5</sub> collected during different monsoon seasons and  
 1510 haze episode in Kuala Lumpur, *Chemosphere*, 219, 1-14, 10.1016/j.chemosphere, 2019.

1511 Tang, Y., Han, G.-L. and Xu, Z.-F.: Characteristics of black carbon content in atmospheric dust in Beijing  
 1512 and its northern regions (in Chinese), *Acta Scientiae Circumstantiae*, 33(02), 332-338,  
 1513 10.13671/j.hjkxxb.2013.02.033, 2013.

1514 Tao, J., Cheng, T., Zhang, R., Cao, J., Zhu, L., Wang, Q., Luo, L., and Zhang, L.: Chemical composition  
 1515 of PM<sub>2.5</sub> at an urban site of Chengdu in southwestern China, *Advances in Atmospheric Sciences*, 30,  
 1516 1070-1084, 10.1007/s00376-012-2168-7, 2013.

1517 Tao, S., Ru, M. Y., Du, W., Zhu, X., Zhong, Q. R., Li, B. G., Shen, G. F., Pan, X. L., Meng, W. J., Chen,  
 1518 Y. L., Shen, H. Z., Lin, N., Su, S., Zhuo, S. J., Huang, T. B., Xu, Y., Yun, X., Liu, J. F., Wang, X. L.,  
 1519 Liu, W. X., Cheng, H. F., and Zhu, D. Q.: Quantifying the rural residential energy transition in China  
 1520 from 1992 to 2012 through a representative national survey, *Nature Energy*, 3, 567-573,  
 1521 10.1038/s41560-018-0158-4, 2018.

1522 Tian, M., Gao, J., Zhang, L., Zhang, H., Feng, C., and Jia, X.: Effects of dust emissions from wind erosion  
 1523 of soil on ambient air quality, *Atmospheric Pollution Research*, 12, 10.1016/j.apr.2021.101108, 2021.

1524 Tian, S. L., Pan, Y. P., and Wang, Y. S.: Size-resolved source apportionment of particulate matter in urban  
 1525 Beijing during haze and non-haze episodes, *Atmospheric Chemistry and Physics*, 16, 1-19,  
 1526 10.5194/acp-16-1-2016, 2016.

1527 Turpin, B. J. and Huntzicker, J. J.: Identification of secondary organic aerosol episodes and quantitation  
 1528 of primary and secondary organic aerosol concentrations during SCAQS, *Atmospheric Environment*,  
 1529 29, 3527-3544, [https://doi.org/10.1016/1352-2310\(94\)00276-Q](https://doi.org/10.1016/1352-2310(94)00276-Q), 1995.

1530 VanCuren, R. and Gustin, M. S.: Identification of sources contributing to PM<sub>2.5</sub> and ozone at elevated  
 1531 sites in the western U.S. by receptor analysis: Lassen Volcanic National Park, California, and Great  
 1532 Basin National Park, Nevada, *Science of The Total Environment*, 530-531, 505-518,

1533 <https://doi.org/10.1016/j.scitotenv>, 2015.

1534 Venkataraman, C., Brauer, M., Tibrewal, K., Sadavarte, P., Ma, Q., Cohen, A., Chaliyakunnel, S., Frostad,  
1535 J., Klimont, Z., Martin, R. V., Millet, D. B., Philip, S., Walker, K., and Wang, S.: Source influence  
1536 on emission pathways and ambient PM<sub>2.5</sub> pollution over India (2015–2050), *Atmospheric Chemistry  
1537 and Physics*, 18, 8017-8039, 10.5194/acp-18-8017-2018, 2018.

1538 Wang, F.: The mechanism and timescales of soil formation in the hyper-arid Atacama Desert, Chile,  
1539 Purdue University, 2013.

1540 Wang, F., Michalski, G., Seo, J.-h., and Ge, W.: Geochemical, isotopic, and mineralogical constraints on  
1541 atmospheric deposition in the hyper-arid Atacama Desert, Chile, *Geochimica et Cosmochimica Acta*,  
1542 135, 29-48, <https://doi.org/10.1016/j.gca>, 2014.

1543 Wang, M., Duan, Y., Xu, W., Wang, Q., Zhang, Z., Yuan, Q., Li, X., Han, S., Tong, H., Huo, J., Chen, J.,  
1544 Gao, S., Wu, Z., Cui, L., Huang, Y., Xiu, G., Cao, J., Fu, Q., and Lee, S.: Measurement report:  
1545 Characterisation and sources of the secondary organic carbon in a Chinese megacity over 5 years  
1546 from 2016 to 2020, *Atmospheric Chemistry and Physics*, 22, 12789-12802, 10.5194/acp-22-12789-  
1547 2022, 2022.

1548 Wei, C., Bandowe, B. A. M., Han, Y., Cao, J., Zhan, C., and Wilcke, W.: Polycyclic aromatic  
1549 hydrocarbons (PAHs) and their derivatives (alkyl-PAHs, oxygenated-PAHs, nitrated-PAHs and  
1550 azaarenes) in urban road dusts from Xi'an, Central China, *Chemosphere*, 134, 512-520,  
1551 <https://doi.org/10.1016/j.chemosphere.2014.11.052>, 2015.

1552 Wei, T., Dong, Z., Kang, S., Qin, X., and Guo, Z.: Geochemical evidence for sources of surface dust  
1553 deposited on the Laohugou glacier, Qilian Mountains, *Applied Geochemistry*, 79, 1-8,  
1554 <https://doi.org/10.1016/j.apgeochem>, 2017.

1555 Wu, C. and Yu, J. Z.: Determination of primary combustion source organic carbon-to-elemental carbon  
1556 (OC/EC) ratio using ambient OC and EC measurements: secondary OC-EC correlation  
1557 minimization method, *Atmospheric Chemistry and Physics*, 16, 5453-5465, 10.5194/acp-16-5453-  
1558 2016, 2016.

1559 Wu, C., Wu, D., and Yu, J. Z.: Quantifying black carbon light absorption enhancement with a novel  
1560 statistical approach, *Atmospheric Chemistry and Physics*, 18, 289-309, 10.5194/acp-18-289-2018,  
1561 2018a.

1562 Xia, X., Zong, X., Cong, Z., Chen, H., Kang, S., and Wang, P.: Baseline continental aerosol over the

1563 central Tibetan plateau and a case study of aerosol transport from South Asia, *Atmospheric*  
1564 *Environment*, 45, 7370-7378, <https://doi.org/10.1016/j.atmosenv.2011.07.067>, 2011.

1565 Xiao, Q., Saikawa, E., Yokelson, R. J., Chen, P., Li, C., and Kang, S.: Indoor air pollution from burning  
1566 yak dung as a household fuel in Tibet, *Atmospheric Environment*, 102, 406-412, [10.1016/j.atmosenv](https://doi.org/10.1016/j.atmosenv.2015.07.067),  
1567 2015.

1568 Xie, F., Guo, L., Wang, Z., Tian, Y., Yue, C., Zhou, X., Wang, W., Xin, J., and Lu, C.: Geochemical  
1569 characteristics and socioeconomic associations of carbonaceous aerosols in coal-fueled cities with  
1570 significant seasonal pollution pattern, *Environmental International*, 179, 108179,  
1571 [10.1016/j.envint.2023.108179](https://doi.org/10.1016/j.envint.2023.108179), 2023.

1572 Xu, L., Chen, X., Chen, J., Zhang, F., He, C., Zhao, J., and Yin, L.: Seasonal variations and chemical  
1573 compositions of PM<sub>2.5</sub> aerosol in the urban area of Fuzhou, China, *Atmospheric Research*, 104-  
1574 105, 264-272, [https://doi.org/10.1016/j.atmosres](https://doi.org/10.1016/j.atmosres.2012.07.012), 2012.

1575 Xu, M., Liu, Z., Hu, B., Yan, G., Zou, J., Zhao, S., Zhou, J., Liu, X., Zheng, X., Zhang, X., Cao, J., Guan,  
1576 M., Lv, Y., and Zhang, Y.: Chemical characterization and source identification of PM<sub>2.5</sub> in Luoyang  
1577 after the clean air actions, *Journal of Environmental Sciences*, 115, 265-276,  
1578 <https://doi.org/10.1016/j.jes.2021.06.021>, 2022.

1579 Xu, R., Tie, X., Li, G., Zhao, S., Cao, J., Feng, T., and Long, X.: Effect of biomass burning on black  
1580 carbon (BC) in South Asia and Tibetan Plateau: The analysis of WRF-Chem modeling, *Science of*  
1581 *The Total Environment*, 645, 901-912, <https://doi.org/10.1016/j.scitotenv.2018.07.165>, 2018b.

1582 Xue, W., Wang, L., Yang, Z., Xiong, Z., Li, X., Xu, Q., and Cai, Z.: Can clean heating effectively alleviate  
1583 air pollution: An empirical study based on the plan for cleaner winter heating in northern China,  
1584 *Applied Energy*, 351, 121923, [https://doi.org/10.1016/j.apenergy](https://doi.org/10.1016/j.apenergy.2023.121923), 2023.

1585 Yan, B., Zheng, M., Hu, Y., Ding, X., Sullivan, A. P., Weber, R. J., Baek, J., Edgerton, E. S., and Russell,  
1586 A. G.: Roadside, urban, and rural comparison of primary and secondary organic molecular markers  
1587 in ambient PM<sub>2.5</sub>, *Environmental Science & Technology*, 43, 4287-4293, [10.1021/es900316g](https://doi.org/10.1021/es900316g), 2009.

1588 Yang, F., He, K., Ye, B., Chen, X., Cha, L., Cadle, S. H., Chan, T., and Mulawa, P. A.: One-year record  
1589 of organic and elemental carbon in fine particles in downtown Beijing and Shanghai, *Atmospheric*  
1590 *Chemistry and Physics*, 5, 1449-1457, [10.5194/acp-5-1449-2005](https://doi.org/10.5194/acp-5-1449-2005), 2005.

1591 Yang, Q.-L., Wang, J.-X. and Zhao, Z.-X.: Temporal and spatial distribution characteristics and source  
1592 analysis of heavy metals in atmospheric dust in typical industrial cities in Northeast China during

1593 winter and spring (in Chinese), *Acta Scientiae Circumstantiae*, 1-9, 10.13671/j.hjkxxb.2024.0254,  
1594 2024.

1595 Yao, L., Yang, L., Yuan, Q., Yan, C., Dong, C., Meng, C., Sui, X., Yang, F., Lu, Y., and Wang, W.: Sources  
1596 apportionment of PM<sub>2.5</sub> in a background site in the North China Plain, *Science of the Total*  
1597 *Environment*, 541, 590-598, 10.1016/j.scitotenv, 2016.

1598 Ye, W., Saikawa, E., Avramov, A., Cho, S. H., and Chartier, R.: Household air pollution and personal  
1599 exposure from burning firewood and yak dung in summer in the eastern Tibetan Plateau,  
1600 *Environmental Pollution*, 263, 114531, 10.1016/j.envpol, 2020.

1601 Yoo, H. Y., Kim, K. A., Kim, Y. P., Jung, C. H., Shin, H. J., Moon, K. J., Park, S. M., and Lee, J. Y.:  
1602 Validation of SOC estimation using OC and EC concentration in PM<sub>2.5</sub> measured at Seoul, *Aerosol*  
1603 *and Air Quality Research*, 22, 210388, 10.4209/aaqr.210388, 2022.

1604 You, S., Yao, Z., Dai, Y., and Wang, C.-H.: A comparison of PM exposure related to emission hotspots in  
1605 a hot and humid urban environment: Concentrations, compositions, respiratory deposition, and  
1606 potential health risks, *Science of The Total Environment*, 599-600, 464-473,  
1607 <https://doi.org/10.1016/j.scitotenv.2017.04.217>, 2017.

1608 Yu, H., Yang, W., Wang, X., Yin, B., Zhang, X., Wang, J., Gu, C., Ming, J., Geng, C., and Bai, Z.: A  
1609 seriously sand storm mixed air-polluted area in the margin of Tarim Basin: Temporal-spatial  
1610 distribution and potential sources, *Science of The Total Environment*, 676, 436-446,  
1611 <https://doi.org/10.1016/j.scitotenv, 2019>.

1612 Yu, L.-P., Li, D., Meng, L., Du, C.-Y. and Zhao, P.: Observation and data processing methods for  
1613 atmospheric dust deposition (in Chinese), *Anhui Agricultural Sciences*, 44: 185-186,  
1614 10.13989/j.cnki.0517-6611.2016.31.064, 2016.

1615 Zhan, C., Han, Y., Cao, J., Wei, C., Zhang, J., and An, Z.: Validation and application of a thermal–optical  
1616 reflectance (TOR) method for measuring black carbon in loess sediments, *Chemosphere*, 91, 1462-  
1617 1470, <https://doi.org/10.1016/j.chemosphere.2012.12.011>, 2013.

1618 Zhan, C.-L., Zhan, J.-W., Ke, Z.-D., Liu, S., Zhang, J.-Q. and Liu, H.-X.: Pollution characteristics and  
1619 source analysis of black carbon in different types of dust in Xiaogan, Hubei (in Chinese),  
1620 *Environmental Pollution and Control* 44(01), 14-19 + 26, 10.15985/j.cnki.1001-3865, 2022.

1621 Zhan, C.-L., Zhang, J.-Q., Zheng, J.-G., Yao, R.-Z., Xiao, W.-S. and Cao, J.-J.: Pollution characteristics  
1622 and source analysis of black carbon in atmospheric dust along National Highway 316 (in Chinese),

1623 Environmental Science and Technology, 39(04), 154-160, 2016.

1624 Zhang, F.: Study on the dry deposition of organic carbon and elemental carbon in the atmosphere of  
1625 Nanchang (in Chinese), Master's Thesis, 2014.

1626 Zhang, F., Wang, Z. W., Cheng, H. R., Lv, X. P., Gong, W., Wang, X. M., and Zhang, G.: Seasonal  
1627 variations and chemical characteristics of PM<sub>2.5</sub> in Wuhan, central China, Science of the Total  
1628 Environment, 518-519, 97-105, 10.1016/j.scitotenv, 2015a.

1629 Zhang, H. and Han, F.: The preliminary remote sensing interpretation of salt lake and its environments  
1630 in the Central Qaidam Basin, Northwest China, Journal of Salt Lake Research, 10, 28-34, 2002.

1631 Zhang, H., Zhang, F., Song, J., Tan, M. L., Kung, H. T., and Johnson, V. C.: Pollutant source, ecological  
1632 and human health risks assessment of heavy metals in soils from coal mining areas in Xinjiang,  
1633 China, Environmental Reserch, 202, 111702, 10.1016/j.envres.2021.111702, 2021a.

1634 Zhang, J., Smith, K. R., Ma, Y., Ye, S., Jiang, F., Qi, W., Liu, P., Khalil, M. A. K., Rasmussen, R. A., and  
1635 Thorneloe, S. A.: Greenhouse gases and other airborne pollutants from household stoves in China:  
1636 a database for emission factors, Atmospheric Environment, 34, 4537-4549,  
1637 [https://doi.org/10.1016/S1352-2310\(99\)00450-1](https://doi.org/10.1016/S1352-2310(99)00450-1), 2000.

1638 Zhang, J., Huang, X., Li, J., Chen, L., Zhao, R., Wang, R., Sun, W., Chen, C., Su, Y., Wang, F., Huang,  
1639 Y., and Lin, C.: Chemical composition, sources and evolution of PM<sub>2.5</sub> during wintertime in the city  
1640 cluster of southern Sichuan, China, Atmospheric Pollution Research, 14, 101635,  
1641 <https://doi.org/10.1016/j.apr.2022.101635>, 2023.

1642 Zhang, K., Shang, X., Herrmann, H., Meng, F., Mo, Z., Chen, J., and Lv, W.: Approaches for identifying  
1643 PM<sub>2.5</sub> source types and source areas at a remote background site of South China in spring, Science  
1644 of The Total Environment, 691, 1320-1327, <https://doi.org/10.1016/j.scitotenv>, 2019.

1645 Zhang, N., Cao, J., Liu, S., Zhao, Z., Xu, H., and Xiao, S.: Chemical composition and sources of PM<sub>2.5</sub>  
1646 and TSP collected at Qinghai Lake during summertime, Atmospheric Research, 138, 213-222,  
1647 <https://doi.org/10.1016/j.atmosres>, 2014.

1648 Zhang, P.-X.: Salt lakes in the Qaidam Basin (in Chinese), Beijing: Science Press, 1987.

1649 Zhang, R., Wang, H., Qian, Y., Rasch, P. J., Easter, R. C., Ma, P. L., Singh, B., Huang, J., and Fu, Q.:  
1650 Quantifying sources, transport, deposition, and radiative forcing of black carbon over the Himalayas  
1651 and Tibetan Plateau, Atmospheric Chemistry and Physics, 15, 6205-6223, 10.5194/acp-15-6205-  
1652 2015, 2015b.

1653 Zhang, X. Y., Wang, Y. Q., Zhang, X. C., Guo, W., and Gong, S. L.: Carbonaceous aerosol composition  
1654 over various regions of China during 2006, *Journal of Geophysical Research: Atmospheres*, 113,  
1655 10.1029/2007jd009525, 2008.

1656 Zhang, X. Y., Wang, Y. Q., Wang, D., Gong, S. L., Arimoto, R., Mao, L. J., and Li, J.: Characterization  
1657 and sources of regional-scale transported carbonaceous and dust aerosols from different pathways  
1658 in coastal and sandy land areas of China, *Journal of Geophysical Research: Atmospheres*, 110,  
1659 10.1029/2004jd005457, 2005.

1660 Zhang, Z., Zhou, Y., Zhao, N., Li, H., Tohniyaz, B., Mperejekumana, P., Hong, Q., Wu, R., Li, G., Sultan,  
1661 M., Zayan, A. M. I., Cao, J., Ahmad, R., and Dong, R.: Clean heating during winter season in  
1662 Northern China: A review, *Renewable and Sustainable Energy Reviews*, 149, 111339,  
1663 [https://doi.org/10.1016/j.rser, 2021b](https://doi.org/10.1016/j.rser.2021b).

1664 Zhang, Z.-C., Xie, Y.-Q., Zhang, Z.-J., Gao, G.-S., Xu, B., Tian, X., Xu, H., Wie, Y.-T., Shi, G.-L. and  
1665 Feng, Y.-C.: Source analysis and seasonal variation characteristics of atmospheric dust deposition  
1666 in Taiyuan City based on two receptor models (in Chinese), *China Environmental Science*, 42, 2577-  
1667 2586, 10.3969/j.issn.1000-6923, 2022.

1668 Zhao, Z., Cao, J., Shen, Z., Xu, B., Zhu, C., Chen, L. W. A., Su, X., Liu, S., Han, Y., Wang, G., and Ho,  
1669 K.: Aerosol particles at a high-altitude site on the Southeast Tibetan Plateau, China: Implications  
1670 for pollution transport from South Asia, *Journal of Geophysical Research: Atmospheres*, 118,  
1671 10.1002/jgrd.50599, 2013.

1672 Zheng, J., Hu, M., Du, Z., Shang, D., Gong, Z., Qin, Y., Fang, J., Gu, F., Li, M., Peng, J., Li, J., Zhang,  
1673 Y., Huang, X., He, L., Wu, Y., and Guo, S.: Influence of biomass burning from South Asia at a high-  
1674 altitude mountain receptor site in China, *Atmospheric Chemistry and Physics*, 17, 6853-6864,  
1675 10.5194/acp-17-6853-2017, 2017.

1676 Zheng, K., Li, Y., Li, Z., and Huang, J.: Provenance tracing of dust using rare earth elements in recent  
1677 snow deposited during the pre-monsoon season from mountain glaciers in the central to northern  
1678 Tibetan Plateau, *Environmental Science and Pollution Research*, 28, 45765-45779, 10.1007/s11356-  
1679 021-13561-x, 2021.

1680 Zheng, M.-P.: Geological report on salt lake resources and ecological environment in China (in Chinese),  
1681 *Acta Geologica Sinica*, 84: 1613-1622. DOI: 10.19762/j.cnki.dizhixuebao, 2017.

1682 Zhou, Y., Gao, X., and Lei, J.: Characteristics of dust weather in the Tarim Basin from 1989 to 2021 and

1683 its impact on the atmospheric environment, 10.3390/rs15071804, 2023.

1684 Zhou, Y., Yang, J., Kang, S., Hu, Y., Chen, X., Xu, M., and Ma, M.: Black carbon aerosols impact  
1685 snowfall over the Tibetan Plateau, *Geoscience Frontiers*, 16, 101978, <https://doi.org/10.1016/j.gsf>,  
1686 2025.

1687 Zhu, C.-S., Chen, C.-C., Cao, J.-J., Tsai, C.-J., Chou, C. C. K., Liu, S.-C., and Roam, G.-D.:  
1688 Characterization of carbon fractions for atmospheric fine particles and nanoparticles in a highway  
1689 tunnel, *Atmospheric Environment*, 44, 2668-2673, 10.1016/j.atmosenv, 2010.

1690 Zhu, H., Li, W., Kong, X., and Zhang, X.: Overlooked contribution of salt lake emissions: A case study  
1691 of dust deposition from the Qinghai-Xizang Plateau, *Journal of Geophysical Research: Atmospheres*,  
1692 130, e2024JD042693, <https://doi.org/10.1029/2024JD042693>, 2025.

1693 Zhu, H.-X.: The dust deposition data of the Qaidam Basin [Data set]. Zenodo.  
1694 <https://doi.org/10.5281/zenodo.14382853>, 2024.